



## The Matuyama–Brunhes reversal in the loess-paleosol sequence of the Otkaznoe section (Terek–Kuma Lowland, Eastern Ciscaucasia)

Varvara I. Dudanova <sup>a,\*</sup>, Evgeny A. Konstantinov <sup>b</sup>, Nikita V. Sychev <sup>b</sup>, Aleksandr M. Pasenko <sup>a</sup>, Pavel G. Panin <sup>b</sup>, Roman V. Veselovskiy <sup>a,c</sup>

<sup>a</sup> Schmidt Institute of Physics of the Earth, Russian Academy of Sciences, B. Gruzinskaya Street 10, 123242, Moscow, Russia

<sup>b</sup> Institute of Geography, Russian Academy of Sciences, Staromonetny 29, 119017, Moscow, Russia

<sup>c</sup> Department of Geology, Lomonosov Moscow State University, Leninskie Gory 1, 119991, Moscow, Russia

### ARTICLE INFO

Handling Editor:

**Keywords:**

Magnetostratigraphy  
Rock magnetism  
Precursor  
Matuyama–Brunhes boundary  
East European Plain  
Lithological analysis

### ABSTRACT

Detailed chronostratigraphy of loess-paleosol sequences (LPSs), based on a multi proxy approach and global correlation with sedimentary records, is essential for Quaternary environmental reconstructions. On the East European Plain, the Eastern Ciscaucasian LPSs are among the longest and the most continuously deposited in Europe. These sequences are comparable to the loess of China and Tajikistan in terms of their stratigraphic completeness and thickness (over 100 m), which allows development of high-resolution records. There, we introduce, for the first time, a comprehensive set of high-resolution data, including paleomagnetic, rock magnetic, grain size, and loss on ignition records, alongside X-ray diffraction and scanning electron microscopy analyses, for the Matuyama–Brunhes (M/B) transition in the Otkaznoe section (Terek-Kuma Lowland), Eastern Ciscaucasia. The M/B transition in the Otkaznoe LPS encompasses a ~1.7 m thick zone, and includes the M/B precursor and the Matuyama–Brunhes boundary (MBB). The precursor to the M/B reversal is recorded in the loess, which correlates with marine isotope stage (MIS) 20, and is characterized by virtual geomagnetic pole (VGP) latitudes of approximately 0°. The MBB in the Otkaznoe section is located in the lower part of the MIS 19 paleosol, rather than in the MIS 20 loess, as was previously assumed. We propose that the M/B precursor in the Otkaznoe section can serve as a reliable chronostratigraphic marker for regional and global correlations, comparable to the M/B boundary. The impact of lock-in processes on the paleomagnetic record of the Otkaznoe section is insignificant.

### 1. Introduction

Cyclical climate variations of the Quaternary period, which are characterized by alternating glacial and interglacial epochs, are recorded in the sequences of loess and paleosols in continental semiarid regions of the temperate zones (Velichko, 1990; Tsatskin et al., 1998; Velichko et al., 2017; Panin et al., 2018, 2023; Kalinin et al., 2024). In contrast to glacial areas, where geological evidence can be lost due to glacial erosion, loess regions experience relatively stable sedimentation, resulting in more complete and continuous geological records. Comprehensive studies of loess-paleosol sequences (LPSs), therefore, provide information about climate variations (Maher, 2016; Cosentino et al., 2024; Alekseev and Alekseeva, 2024), geomagnetic field changes (Fan et al., 2024), paleowind directions (Lagroix and Banerjee, 2004; Zhang et al., 2010; Ge et al., 2014; Bradak et al., 2019; Mazneva et al.,

2021), and paleogeographic conditions (Velichko et al., 2007, 2012; Pye, 1995). Detailed chronostratigraphy of LPSs, along with their correlation to both marine and continental sedimentary records on regional and global scales, forms the basis for environmental reconstructions over the past 2.6 Myr and beyond. Stable plateau-like LPSs with increased thickness are especially valuable for chronostratigraphy, because they can preserve loess and paleosol horizons, with spatial stability in sediment structure and high-resolution (Marković et al., 2018).

The LPSs of the Terek-Kuma Lowland (Eastern Ciscaucasia) are among the most extensive, exceeding 100 m in thickness, and stratigraphically complete in Europe (Andreeva et al., 2008), comparable to the loess cover of China and Central Asia (Kukla and An, 1989; Dodonov, 1991; Bronger, 2003). A notable and easily accessible loess-paleosol profile in the Terek-Kuma Lowland is the Otkaznoe section (Fig. 1a and b). Despite its potential for providing valuable insights and a long

\* Corresponding author.

E-mail address: [varvara.dudanova@mail.ru](mailto:varvara.dudanova@mail.ru) (V.I. Dudanova).

## Abbreviations

LPS	loess-paleosol sequence
MIS	marine isotope stage
MBB	Matuyama-Brunhes boundary
MBR	Matuyama-Brunhes reversal
NRM	natural remanent magnetization
VGP	virtual geomagnetic pole
AMS	anisotropy of magnetic susceptibility
XRD	X-ray diffraction
SEM	scanning electron microscopy
LOI	loss on ignition
PCA	principal component analysis
ChRM	characteristic remanent magnetization
VRM	viscous remanent magnetization
ARM	anhydrous remanent magnetization
RPI	relative paleointensity

history of investigation, existing stratigraphic schemes for the Otkaznoe section (Udartsev et al., 1989; Galay, 1992; Morozov, 1989; Bolikhovskaya, 1995; Bolikhovskaya et al., 2016; Faustov and Virina, 2001) are largely inconsistent. This discrepancy primarily arises from a lack of reliable geochronological data. Although recent advances in geochronological studies of the Otkaznoe section (Sychev et al., 2022; Ponomareva et al., 2023) have been made, the chronostratigraphic division of the Lower-Middle Pleistocene loess-paleosol sequence continues to be debated.

A reliable approach to developing a chronostratigraphy can be provided by high-resolution paleomagnetic research. The Matuyama-Brunhes reversal (MBR) – the last magnetic polarity transition – represents one of the most significant and widely used Quaternary chronostratigraphic markers. It has been suggested that the geomagnetic reversal has a complex structure characterized by three consecutive phases: precursor, polarity switch and rebound (Valet et al., 2012). The accepted age of the Matuyama-Brunhes boundary (MBB), i.e. the polarity switch, is estimated to be 773 ka (Singer et al., 2019; Channell et al., 2020) or 770–780 ka (Mahgoub et al., 2023). The precursor event is estimated to fall between 785 and 800 ka (Mahgoub et al., 2023). The MBB occurs in marine isotope stage (MIS) 19, and the precursor (794 ka) coincides with the MIS 19/20 boundary or the end of MIS 20 (Channell et al., 2020). Estimates of the transition duration range from approximately 10 ka (Valet et al., 2012) to 22–30 ka (Singer et al., 2019; Mahgoub et al., 2023).

In the Otkaznoe section, the MBR was initially identified by Faustov and Virina (2001) in three cores (no. 3, 6, 18) at a depth of ~75 m beneath the surface of the loess plateau (Fig. 1b). These data were obtained from non-oriented by declination cores with a resolution of 0.5–2.0 m. Incomplete thermal demagnetization (to 200–300 °C) was performed for the specimens. Further, based on this definition, Bolikhovskaya et al. (2016) correlated the MBB in the Otkaznoe section with the end of MIS 20, which is not in agreement with the marine paleomagnetic records (Channell et al., 2020). The results obtained by Faustov and Virina (2001) and Bolikhovskaya et al. (2016) highlight the necessity of re-examine the Otkaznoe section with modern methodological standards for laboratory processing of paleomagnetic data (Tauxe, 2010).

New high-resolution magnetostratigraphic research of the Otkaznoe section, previously performed within Brunhes chron by our group, has revealed a new chronostratigraphic marker – Big Lost excursion (Dudanova et al., 2025) – confirming the potential for conducting detailed investigations of the geomagnetic field changes. The aim of this research is to obtain a high-resolution paleomagnetic record of the M/B transition and to establish the precise stratigraphic position of the MBB

in the Otkaznoe section. To accomplish this, we conducted detailed magnetostratigraphic investigations with high sampling resolution – specimens were taken at 2 cm stratigraphic intervals. We also made grain size, rock magnetic, loss on ignition (LOI), and magnetic mineralogy analyses, including scanning electron microscope (SEM) observation and X-ray diffraction (XRD) analyses.

## 2. Materials and methods

### 2.1. The studied section

The Otkaznoe section is located in the Eastern Ciscaucasia on the high right bank of the Kuma River, approximately 2.8 km south of the Otkaznoe village, within the Terek-Kuma Lowland. The construction of the Otkaznoe reservoir in the 1960s led to the creation of steep cliffs along the banks, revealing over 50 m of Quaternary LPS (Fig. 1b and c). Additionally, a large quarry was established (N 44°17'59", E 43°51'51"), providing a clear exposure of loess deposits. Extensive research of the Otkaznoe section was conducted in the second half of the 1980s (Udartsev et al., 1989; Morozov, 1989; Galay, 1992; Bolikhovskaya, 1995; Faustov and Virina, 2001). As a result, a series of boreholes and sections in the quarry and coastal outcrops of the Otkaznoe reservoir were studied, revealing a loess and loess-like deposits with a thickness of 140 m. Since the bottom of the quarry (178 m a.s.l.) was located above the Matuyama-Brunhes boundary, paleomagnetic studies (Faustov and Virina, 2001) were carried out on core samples from borehole no. 6, which was drilled at the bottom of this quarry. In this research we studied a quarry wall (OT-23-10), located 400 m south (N 44°17'47", E 43°51'44") of borehole no. 6 (Fig. 1d), which exposes loess-paleosol deposits at lower altitudes of 183–172 m a.s.l. The edge of these outcrops was taken as the relative zero reference point (Fig. 1d).

### 2.2. Sampling

To obtain a detailed rock magnetic and paleomagnetic data on the Matuyama-Brunhes transition in the Otkaznoe section, we conducted continuous sampling of oriented blocks from section OT-23-10 (Fig. 1d and e). The sampled interval had a thickness of 9.5 m. Paleomagnetic samples were prepared as blocks measuring 15 × 10 × 8 cm, which were cut from the subvertical walls of the section (Fig. 1f). A total of 74 blocks were collected, each oriented with a magnetic compass. In the laboratory, we used a stone-cutting machine equipped with a diamond disc to slice the blocks into horizontal (stratigraphic) levels, each 2 cm thick. These levels were then further cut into standard paleomagnetic cube specimens measuring 2 × 2 × 2 cm. For each stratigraphic level we obtained between 2 and 6 duplicate sister-specimens. Ultimately, paleomagnetic collection comprised 1102 specimens representing 269 stratigraphic levels. Samples for lithological analysis were collected without gaps with a step of 10 cm. The sampling interval was from 8.00 to 18.60 m. A total of 107 samples were collected.

### 2.3. Methods

Laboratory rock magnetic and paleomagnetic measurements were conducted following standard methods (Tauxe, 2010) at the Schmidt Institute of Physics of the Earth, Russian Academy of Sciences (Laboratory for Main Geomagnetic Field and Rock Magnetism, Moscow) using the equipment from Shared Research Facilities (Veselovskiy et al., 2022) and at the Lomonosov Moscow State University (Laboratory for Rock Magnetism, Faculty of Geology, Moscow).

#### 2.3.1. Paleomagnetism

We carried out progressive thermal (TH) and alternating field (AF) demagnetization on 329 and 773 specimens, respectively. AF demagnetization involved 12 to 15 steps, reaching up to 110–130 mT, and was performed on 2–5 specimens from each stratigraphic level using a

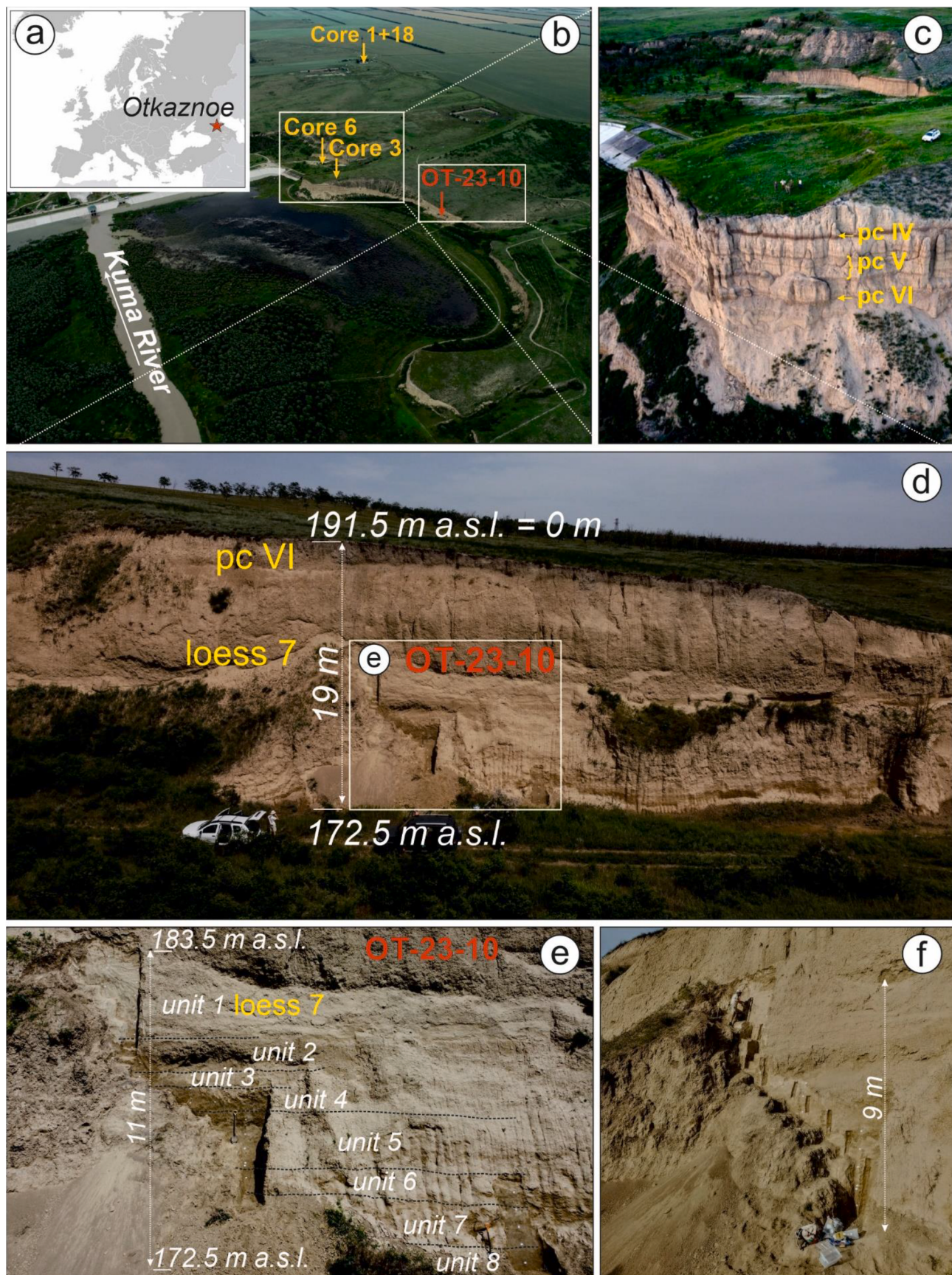


**Fig. 1.** Location of the Otkaznoe section (a); (b-c) general view of the outcrop on the SE wall of the Otkaznoe reservoir. The yellow arrows in (b) indicate previous core drilling sites (Bolikhovskaya et al., 2016) and the red arrow indicates the studied outcrop location (d-e); general and detailed view of the OT-23-10 section; (f) sampling of oriented blocks for paleomagnetic study. PC IV, V, VI and loess 7 are labelled according to the lithological and paleosol investigations presented here.

demagnetizer attached to a superconducting rock magnetometer (2G Enterprises, USA). During TH demagnetization specimens were stepwise (8–12 steps) heated to 590–690 °C in a MMTD80 non-magnetic oven (Magnetic Measurements, UK), with 1–3 specimens from each level being treated (except for the upper 2 m of the section, where only AF demagnetization was applied to all specimens). NRM for thermally demagnetized specimens was measured using a JR-6 spin-magnetometer (AGICO, Czech Republic); a superconducting rock magnetometer, installed in a shielded room (Lodestar Magnetics, USA), was used for AF demagnetization. Demagnetization results were analyzed using the PMTools software (Efremov and Veselovskiy, 2023).

For each specimen, the direction of the characteristic remanent magnetization (ChRM) was determined using principal component analysis (PCA) (Kirschvink, 1980). PCA results for duplicate specimens from the same stratigraphic level were averaged. Mean ChRM directions were calculated employing Fisher statistics (Fisher, 1953). Specimens with statistically significant different ChRM directions (>45°) compared to other sister-specimens from the same level were excluded from calculation of the ChRM directions. To evaluate the quality of the paleomagnetic signal within each stratigraphic level, we determined the maximum angular deviation (MAD), which was calculated as the arithmetic mean of the MAD of all duplicate specimens from a single level (Kulakova and Kurbanov, 2023). Magnetic polarity was distinguished based on virtual geomagnetic pole (VGP) latitude. Normal polarity was identified when VGP latitude >45°, while reverse polarity is indicated by VGP latitude <−45°. VGP latitudes between −45° and 45° are considered anomalous (transitional polarity).

In addition to the paleomagnetic directions, we obtained normalized remanence records, which were calculated as the ratios  $NRM_{300}/\chi$ ,  $NRM_{35 \text{ mT}}/\chi$ ,  $NRM_{35 \text{ mT}}/ARM_{35 \text{ mT}}$  and  $\Delta NRM/\Delta ARM$ , where:

$NRM_{300}$  is the NRM after 300°C TH demagnetization,

$NRM_{35 \text{ mT}}$  ( $ARM_{35 \text{ mT}}$ ) is the NRM (ARM) after AF demagnetization up to 35 mT, and.

$$\Delta NRM = NRM_{26 \text{ mT}} - NRM_{70 \text{ mT}}, \Delta ARM = ARM_{26 \text{ mT}} - ARM_{70 \text{ mT}}.$$

We used a standard temperature of 300 °C and an AF of 35 mT, due to the fact that the ChRM is reliably defined at these demagnetization steps. The difference in the partial NRM (ARM) of 26–70 mT represents the mean demagnetization range of the characteristic component. ARM was produced in a DC field of 65 µT and a maximum AF of 110 mT using a magnetizer attached to superconducting rock magnetometer (2G Enterprises, USA) and subsequently was stepwise (in 13 steps) AF demagnetized up to 110 mT.

### 2.3.2. Rock magnetic measurements

Bulk magnetic susceptibility was measured using a MFK-1A Kappabridge (AGICO, Czech Republic) at dual frequencies of 976 Hz ( $\chi_{lf}$ ) and 15616 Hz ( $\chi_{hf}$ ) with a 200 A/m field for one specimen from every stratigraphic level. All measurements were normalized by mass. Frequency dependence of susceptibility ( $\Delta\chi$ ,  $\chi_{fd}$ ) was determined as follows:

$$\Delta\chi \left[ \frac{\text{m}^3}{\text{kg}} \right] = \chi_{lf} - \chi_{hf}$$

and

$$\chi_{fd} [\%] = \frac{\chi_{lf} - \chi_{hf}}{\chi_{lf}} \times 100.$$

The anisotropy of magnetic susceptibility (AMS) of cube specimens was also measured with a MFK-1A kappabridge (AGICO, Czech Republic) before demagnetization. The AMS is generally described by an oriented ellipsoid with maximum ( $K_1$ ), intermediate ( $K_2$ ) and minimum ( $K_3$ ) axes of magnetic susceptibility (Jelinek, 1981). Parameters of the AMS ellipsoid – corrected degree of anisotropy ( $P_j$ ), shape factor ( $T$ ), lineation ( $L$ ) and foliation ( $F$ ) – were obtained with the Anisoft 6.0 software (AGICO). To ensure the accurate interpretation of the data, we applied filtering technique (Lagroix and Banerjee, 2004; Zhu et al.,

2004). These filters are commonly used in AMS studies of loess-paleosol sequences (e.g., Zhang et al., 2010; Ge et al., 2014; Niezabitowska et al., 2024). We used the filters  $F_{12} > 4$  and  $F_{23} > 10$ , as suggested by Zhu et al. (2004), to evaluate the statistical significance of the lineation and foliation. The equality to orientations of the AMS principal axes was defined by  $\varepsilon_{12} < 22.5^\circ$ , where  $\varepsilon_{12}$  represents the half-angular uncertainty in the direction of  $K_1$  in the plane joining  $K_1$  and  $K_2$  within a 95 % confidence interval (Lagroix and Banerjee, 2004; Zhu et al., 2004). We also applied the filter  $I-K_3 > 70^\circ$  to assess the undisturbed magnetic fabric in sediments, where  $I-K_3$  is the inclination of minimum axis distributed along the vertical axis of the stereoplot (Zhang et al., 2010).

Temperature dependence of magnetic susceptibility ( $\chi-T$ ) was traced using a KLY-4S system equipped with a CS-3 furnace (AGICO, Czech Republic) at 875 Hz and a field of 435 A/m. Powdered samples were heated in air to 700 °C and subsequently cooled to room temperature (heating/cooling rate of 10°C/min). Hysteresis loops, isothermal remanent magnetization (IRM) and backfield acquisition curves for 30 representative samples were obtained using a PMC MicroMag 3900 VSM (LakeShore, USA) with a maximum applied field of 1.0 T. Measurements were normalized by sample mass and corrected for the paramagnetic component.

### 2.4. Grain size analysis and loss on ignition (LOI)

Grain size analysis was conducted using a Malvern Mastersizer 3000 Laser Particle Analyzer (Malvern Panalytical, UK) equipped with a Hydro EV unit at the Institute of Geography of the Russian Academy of Sciences (Environment Paleoarchives Laboratory, Moscow, Russia). Sample preparations were performed following Konert and Vandenberghe (1997), Varga et al. (2019) and Blott et al. (2004). Samples were treated with HCl (10 %) to dissolve carbonates and  $H_2O_2$  (30 %) to remove organic matter. Samples were then mixed in an overhead shaker for 12 h in a 4 %  $Na_4P_2O_7$  solution, sonicated in an ultrasonic bath for 30 min, dispersed in the Hydro EV unit with stirrer mixing (2700 rpm) and built-in ultrasound (50 s), and subsequently measured seven times. Results were averaged using Mastersizer software v. 3.62. To calculate the particle size distribution, we used Mie theory, with values of the refractive index of the particles  $n = 1.55$  and the absorption coefficient  $k = 0.1$  (Ozer et al., 2010).

LOI was conducted to evaluate the organic matter and carbonates contents in the sediment. According to Heiri et al. (2001) and Bengtsson and Enel (1986), the LOI at 550 °C indicates the amount of organic matter, while the difference between LOI at 950 °C and LOI at 550 °C represents the loss of  $CO_2$  from carbonates. Samples (10 ml each) were dried for 12 h at 105 °C to eliminate hygroscopic moisture. Subsequently, ignition was performed in a muffle furnace at two temperature settings (4 h at 550 °C and 2 h at 950 °C). Weight losses were determined by reweighing on electronic scales with an accuracy of 0.01 g. Resulting values were calculated as follows:

$$LOI_{550} (\%) = \frac{DW_{105} - DW_{550}}{DW_{105}} \times 100$$

$$LOI_{\Delta 950} (\%) = \frac{DW_{550} - DW_{950}}{DW_{105}} \times 100, \text{ where } DW = \text{dry weight}$$

The  $CaCO_3$  content was estimated using the formula  $LOI_{\Delta 950} \times 0.44$  (Dean, 1974).

### 2.5. Scanning electron microscopy (SEM) and X-ray diffraction analysis (XRD)

Magnetic minerals were characterized using XRD and SEM. The XRD analysis was performed at the «Borok» Geophysical Observatory (Yaroslavl Region, Russia). The magnetic fraction of the samples was analyzed using a multifunctional powder X-ray spectrometer STADI-MP (STOE, Germany). Diffraction peaks were compared with reference

values from the ICDD PDF-2 powder diffraction database (Gates-Rector and Blanton, 2019). The magnetic fraction was observed using a Tescan Mira LMS IV SEM (Czech Republic) equipped with back-scattered electron (BSE) detectors and an Ultim Max 65 energy dispersive X-ray spectrometer (EDX) with integrated AZtecLive Automated software (Oxford Instruments, UK). To apply a carbon coating to the powder sample, a Q150R ES Plus (Quorum Technologies) automatic sputtering system was utilized. Imaging was conducted at a working distance of 15 mm with an accelerating voltage of 20 keV and a probe current of 3 nA.

### 3. Results

#### 3.1. Loess-paleosol stratigraphy and lithological analysis

Lithostratigraphic subdivision into units 1–8 (Fig. 2a–e) of the OT-23-10 section was achieved based on field description (Fig. 2a–c), grain size (Fig. 2f and g) and LOI (Fig. 2h and i) analyses. Loess horizons (units 1, 3, 5, 7), represented by dark pale, non-layered carbonate-rich material with a predominance of silt fraction (66–76 %) and small Fe-Mn concretions, are dominant. Some loess horizons are sandy

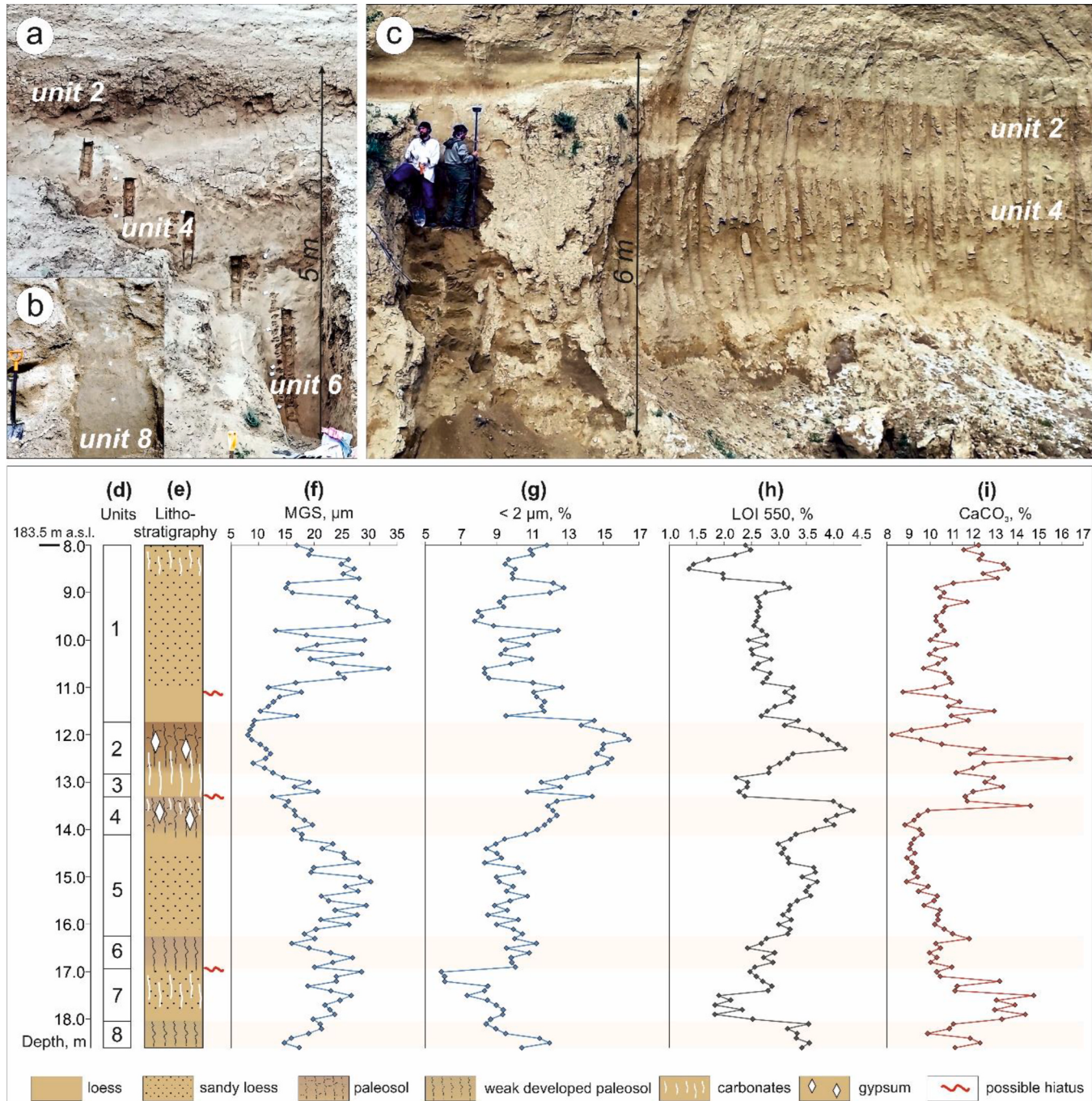


**Fig. 2.** Loess-paleosol stratigraphy of the Otkaznoe section (OT-23-10): (a–c) photos of paleosol (a, b – main section (photo 2023), paleosols (units 2, 4, 6, 8) are expressed by a slightly darker color and columnar jointing, which is especially visible on the dry wall; c – old section (photo 2021), located 60 m south of the main one, paleosols (units 2 and 4) are clearly visible on the fresh wall); (d) lithological units; (e) lithostratigraphy and (f–i) lithological properties: (f) median grain size (MGS); (g) clay content; (h) loss on ignition (LOI 550); (i) carbonates content. 183.5 m a.s.l. – meters from the edge of the cliff. Paleosol units on graphs are represented by a pale.

(Fig. 2e): in these intervals, the sand fraction proportion ( $>63 \mu\text{m}$ ) exceeds 15 %. The clay fraction ( $<2 \mu\text{m}$ ) in loess horizons varies from 6 to 13 % (Fig. 2g).

Paleosol of units 2 and 4 are clearly visible on the fresh outcrop by their pale-brown color, and on the dried outcrop wall by characteristic cracking that forms vertical columnar jointing (Fig. 2a–c). These paleosols have a cloddy-granular structure and are associated with an increased clay fraction (10–16 %) in the 11.80–14.10 m interval (Fig. 2g). In the lower part of these paleosols carbonate horizons occur with a  $\text{CaCO}_3$  content of 13–16 % (Fig. 2i). In paleosols of units 2 and 4, scattered microcrystals of gypsum and single gypsum roses are observed. LOI 550 peaks in units 2 and 4 (Fig. 2h) are likely partly related to the presence of gypsum, which loses water upon ignition.

The paleosol of unit 6 is light brown and has relatively low clay content (9–11 %). In the humus horizon, comparatively low carbonate content (10 %) is recorded, while in the upper part of unit 7, carbonate content increases to 13–15 % (Fig. 2i). Unit 8 is a weakly developed paleosol, with slight darkening, increased clay fraction, increased LOI 550, and lower carbonate content (Fig. 2h and i). Based on sharp changes in sediment characteristics, primarily in the grain size composition, we also identified proposed hiatuses in sediment accumulation, indicated by red wavy lines in Fig. 2e.

### 3.2. Magnetic susceptibility and AMS

$\chi_{lf}$ ,  $\Delta\chi$ , and  $\chi_{fd}$  variations for units 1–8 are shown in Fig. 3c–e. Contrary to expectations, the paleosol does not have higher magnetic susceptibility and frequency dependence compared to the loess. The magnetic enhancement model, based on a systematic increase in  $\chi_{lf}$  and  $\chi_{fd}$  in paleosols due to superparamagnetic (SP) grains of magnetite or maghemite contribution that formed during pedogenesis (Bradak et al., 2021), is typical of most loess-paleosol sequences in the Chinese Loess Plateau (CLP) and Europe (Heller et al., 1993; Liu et al., 2004; Maher, 2011). In contrast, for the Alaska and Siberia LPS, the opposite wind-vigour model is characteristic, in which high  $\chi_{lf}$  occurs in loess and

$\chi_{lf}$  is low in paleosols (Beget and Hawkins, 1989; Liu et al., 1999, 2008).

In the studied Otkaznoe section sequence, the highest  $\chi_{lf}$  values occur in unit 1, while the lowest  $\chi_{lf}$  values are observed in loess unit 5 and paleosol unit 8 (Fig. 3c). Paleosol units generally exhibit relatively low  $\chi_{lf}$ . Small positive peaks of  $\chi_{lf}$  at depths of 13.00 and 17.20 m are confined to the boundary between loess and paleosol units 2/3 and 6/7, respectively. Maximum  $\chi_{lf}$  of  $93.4 \times 10^{-8} \text{ m}^3/\text{kg}$  recorded at 11.10 m as a sharp positive peak. The frequency dependence of magnetic susceptibility ( $\Delta\chi$ ,  $\chi_{fd}$ ), which can provide information about the superparamagnetic (SP) grain concentration, generally decreases monotonically from unit 8 to unit 5, increases in units 2–4, and has consistently high values of  $\Delta\chi$  and  $\chi_{fd}$  in unit 1 (Fig. 3d and e). The maximum frequency dependence is observed in loess unit 1 (4.4 %) and paleosol unit 2 (4.3 %). This suggests a greater presence of ultrafine magnetic particles in these units, in contrast to the top of unit 5 and its boundary with unit 4, where SP grains are almost absent. These data cannot be explained fully by either pedogenic enhancement or wind-vigour models, which apparently indicates that additional regional factors influence the relationship between  $\chi_{lf}$  and  $\chi_{fd}$  and lead to relatively high  $\chi_{fd}$  values in the loess unit 1. For instance, Bradak et al. (2021) pointed out several factors, including surface oxidation of coarse magnetic grains (detrital magnetic enhancement), nanofragmentation by physical weathering, and the appearance of significant ultrafine magnetic inclusions in micas.

In the Otkaznoe section, a sharp  $\chi_{lf}$  and  $\Delta\chi$  peak along with a  $\chi_{fd}$  increase, identified at 9.00–11.10 m, corresponds to sandy loess unit 1. In this interval, the notable magnetic susceptibility rise is accompanied by a NRM increase (Fig. 3f), which may indicate a significant magnetic minerals concentration increase.

AMS results for 151 specimens from units 1–8 are shown in Fig. 4a and b. The sediments have a typical sedimentary magnetic fabric: minimum axes have nearly vertical directions, and maximum and intermediate axes are nearly horizontal and distributed around a great circle (Fig. 4b). 134 specimens (88.7 %) meet all statistically relevant filters. Specifically, the filter  $I-K3 > 70^\circ$  is satisfied by 97.4 % of

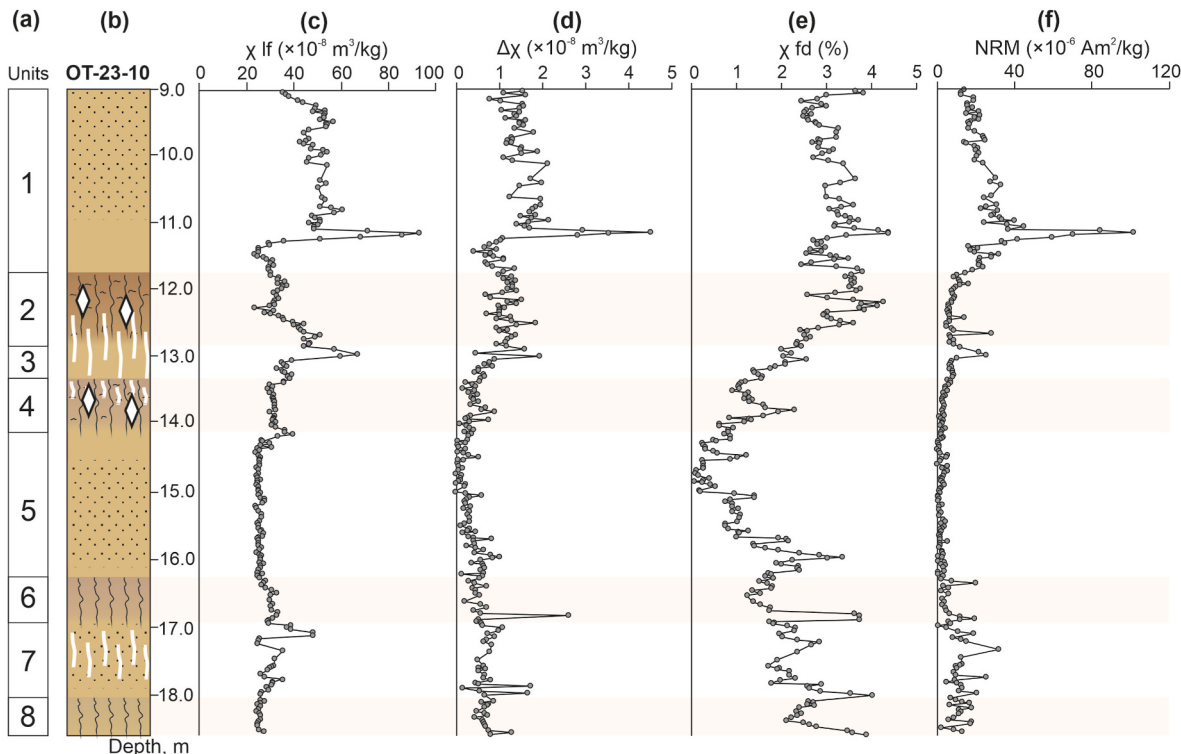
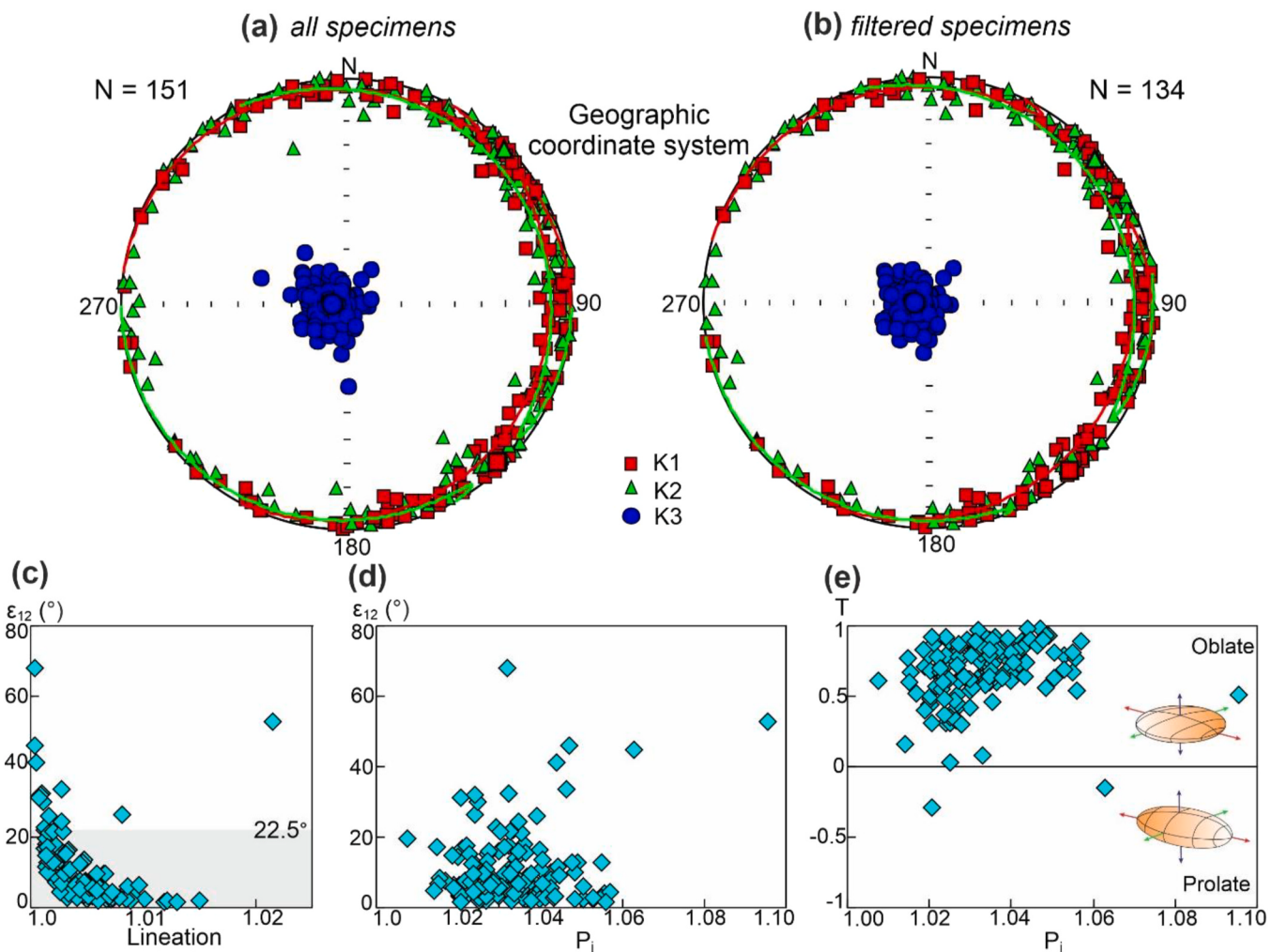


Fig. 3. Lithological units (a), lithostratigraphy (b) and magnetic susceptibility parameters for the Otkaznoe section: (c) low-frequency magnetic susceptibility measured at 976 Hz; (d) absolute and (e) the percent frequency dependence of magnetic susceptibility and (f) natural remanent magnetization.



**Fig. 4.** AMS results for the Otkaznoe section: (a) all specimens; (b) after filtering according to Lagroix and Banerjee (2004) and Zhu et al. (2004). Plots of the relationship between different AMS parameters: (c) lineation (L) and  $\varepsilon_{12}$ ; (d) corrected degree of anisotropy ( $P_j$ ) and  $\varepsilon_{12}$ ; (e)  $P_j$  and shape parameter of AMS ellipsoid (T).

specimens, with an average I-K<sub>3</sub> value of 84.8°, which suggests that the magnetic fabric is primary. The parameter  $\varepsilon_{12}$  has an expected inverse relationship with the magnetic lineation, while no correlation is observed between  $\varepsilon_{12}$  and  $P_j$  (Fig. 4c and d).  $P_j$  is mainly 2–6 %, occasionally reaching 10 % (Fig. 4e). Most specimens have an oblate ( $T > 0$ ) susceptibility ellipsoid, which is typical for loess. These results suggest a primary undisturbed magnetic fabric of the loess and paleosol units.

### 3.3. Hysteresis properties

Hysteresis loops, IRM and backfield acquisition curves for representative loess and paleosol samples from units 1–8 are presented in Fig. 5a–c. Hysteresis loops are closed before 300 mT, and IRM acquisition curves show that samples reach 90 % of the saturation isothermal remanent magnetization (SIRM) before 200 mT. Backfield demagnetization curves observe that the  $B_{cr}$  range from 30.5 to 34.3 mT. The data suggest that low-coercivity soft magnetic minerals dominate both loess and paleosol units.

### 3.4. Magnetic mineralogy

X-ray diffraction analysis (XRD) indicates that the magnetic fraction in loess and paleosol samples from the Otkaznoe section comprises low-titanium titanomagnetite ( $a = 8.40 \text{ \AA}$ ; 29.8–52.6 %) and single-phase oxidized magnetite ( $a = 8.367 \text{ \AA}$ ; 24.6–30.7 %). Hematite ( $a = 5.055$

$\text{\AA}$ ,  $c = 13.726 \text{ \AA}$ ; 15.5–36.9 %) and hemoilmenite ( $a = 5.069 \text{ \AA}$ ,  $c = 13.950 \text{ \AA}$ ; 4.4–6.1 %) are also indicated.

Representative  $\chi$ -T heating curves reveal a sharp  $\chi(T)$  decrease at ~560–580 °C (Fig. 5d–i) for all samples, which indicates the presence of magnetite (or low-Ti titanomagnetite). An ongoing  $\chi(T)$  decrease to 700 °C likely suggests the presence of hematite in both loess and paleosols, consistent with XRD results. The slight  $\chi(T)$  increase to 300 °C with a turning point at 310–320 °C, most prominently observed in paleosol samples (Fig. 5f–h), may be associated with the transformation of iron-containing hydroxides (goethite) and silicate minerals to hematite/magnetite during heating. This laboratory formation of magnetite/hematite from paramagnetic minerals accounts for the sharp  $\chi(T)$  increase (1.5–2 times) observed in  $\chi$ -T cooling curves (Deng et al., 2000).

Scanning electron microscopy of loess powder samples reveals that the magnetic fraction contains both well-preserved titanomagnetite crystals (Fig. 6c–f) and grains with signs of mechanical abrasion (Fig. 6d). Individual isometric rounded titanomagnetite grains are also identified (Fig. 6e). Heterophase oxidation structures are frequently observed in the titanomagnetites (Fig. 6b–e), along with apatite inclusions (Fig. 6a–d), which indicate a primary magmatic origin for these magnetic grains. These findings suggest that the magnetic minerals in loess are detrital in nature.

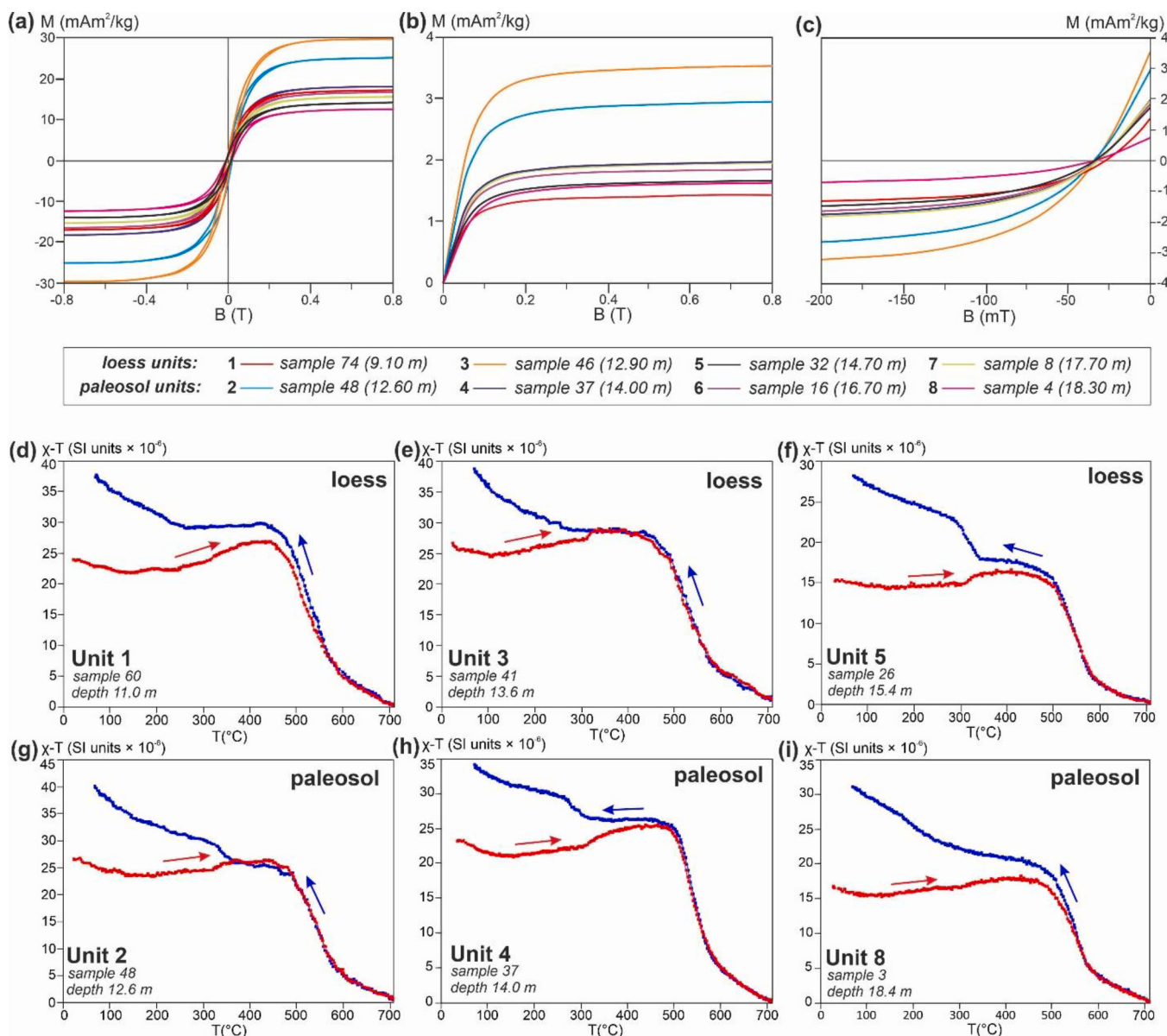


**Fig. 5.** Hysteresis parameters for representative loess and paleosol samples: (a) hysteresis loops, (b) IRM and (c) backfield acquisition, and (d–i) temperature dependence of magnetic susceptibility ( $\chi-T$ ) curves.

### 3.5. Paleomagnetic directions

Representative Zijderveld (1967) diagrams, stereograms and demagnetization intensity plots are shown in Fig. 7. NRM intensity varies considerably, ranging from 0.6 to  $101.7 \times 10^{-6}$  Am<sup>2</sup>/kg (Fig. 3f). NRM is typically a sum of two components: (1) a low-coercivity/low-temperature component that is removed before 11–20 mT or up to 180 °C, likely viscous in nature; and (2) a high-coercivity/high-temperature characteristic (ChRM) component with either normal or reverse polarity. The ChRM component is separated between 20 and 26 and 110 mT or 250–590 °C. We refer to the ChRM as the one directed toward the origin in the Zijderveld (1967) diagram. ChRM directions, identified from TH and AF demagnetizations, are largely consistent (Fig. 7a and b).

Thermal demagnetization completely removes the characteristic component between 590 and 690 °C. In contrast, AF demagnetization to 80–90 % of initial values at 110–130 mT further supports the presence of a high-coercivity magnetic mineral.

Paleomagnetic directions (declination and inclination of ChRM) and

VGP latitudes, calculated from component analysis of 269 stratigraphic levels with averaging of duplicate specimens from each level, are shown in Fig. 8c–e. Units 1–3 and the main part of unit 4, carry a stable normal polarity ChRM, while in units 5–8 a reverse polarity ChRM is observed. The polarity reversal at 14.06 m can be correlated unequivocally with the MBB. Thus, the MBB in the Otkaznoe section is recorded at the base of paleosol unit 4 (Fig. 8).

In unit 5, at 15.17–15.80 m, two closely positioned zones with anomalous paleomagnetic directions are clearly distinguished (Fig. 8g). The r1a zone encompasses an interval of 0.4 m thickness (13 stratigraphic levels) with declinations near 0° and VGP latitudes ranging from –30° to 0°. The r2a zone consists of 4 stratigraphic levels (15.17–15.28 m) with VGP latitudes close to –45° to –40°. At the boundary between units 5 and 6 (16.33 m), there is only one stratigraphic level with transitional polarity. Therefore, it is not distinguished as a separate magnetic polarity zone. The r3a zone, identified at 14.06–14.35 m (9 stratigraphic levels), contains individual levels with normal or reverse polarity and VGP latitudes < –45°, as well as the noisiest paleomagnetic record, which, in some cases, leads to an inability to isolate a ChRM

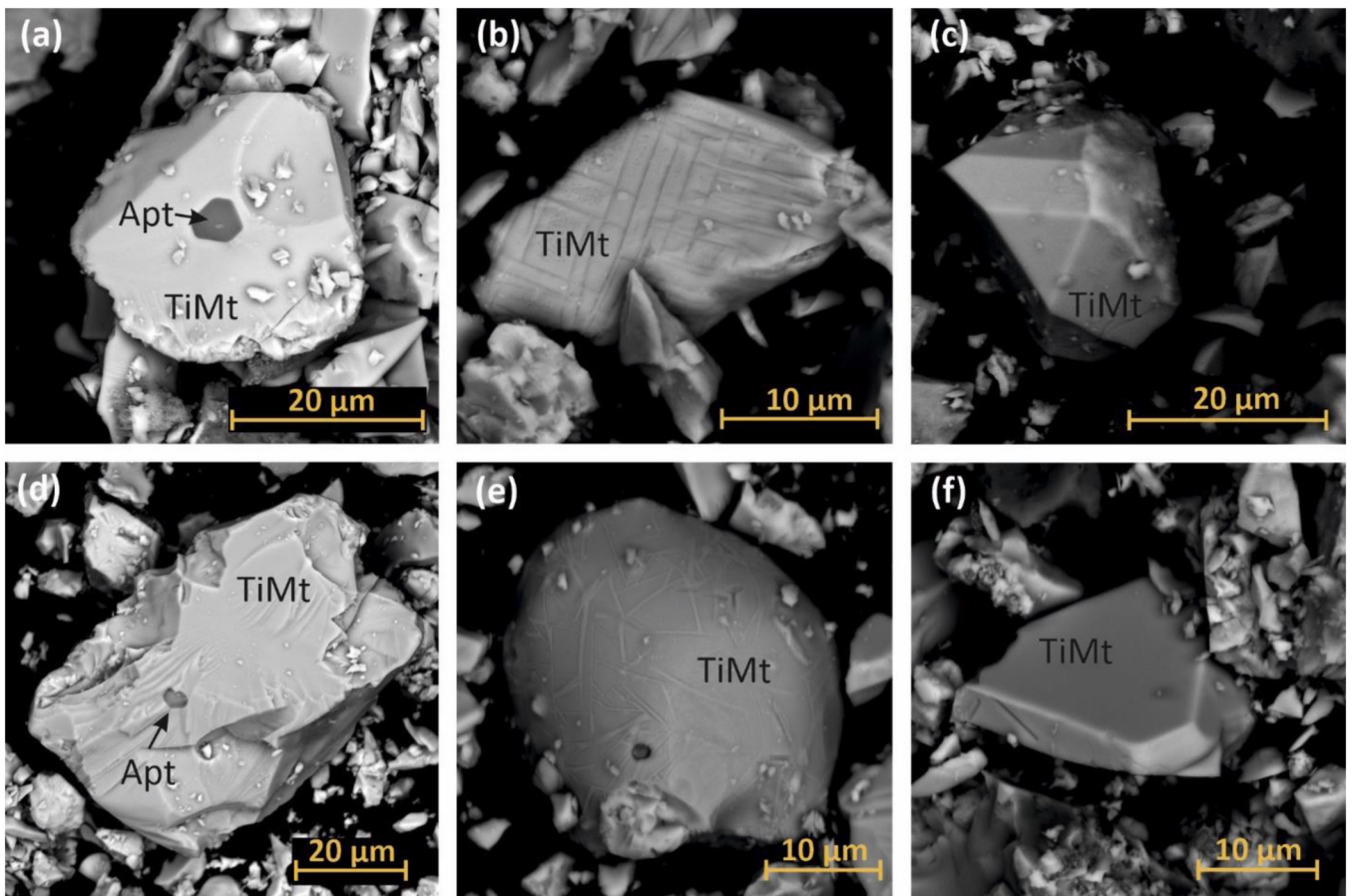


**Fig. 6.** Scanning electron microscopy (SEM): back-scattered electron (BSE) images of titanomagnetite grains from unit 5, sample 35a, depth 14.30 m. TiMt – titanomagnetite; Apt – apatite.

(Fig. 7d).

The interval from 14.06 to 15.80 m represents a transition zone from stable reverse to stable normal polarity. For this interval, higher MAD values are observed (Fig. 8f), indicates a deterioration in paleomagnetic recording quality. Mean MAD value in this interval is  $5.7^\circ$ . Maximum value of mean MAD is  $12.2^\circ$ , while individual MADs can reach up to  $18^\circ$ . For stable normal/reverse polarity intervals, the mean MAD value is  $2.9^\circ/3.1^\circ$ .

The ChRM direction distribution, averaged for each stratigraphic level (Fig. A.1), has an antipodal pattern with a positive reversal test:  $\gamma/\gamma_{cr} = 3.61^\circ/3.92^\circ$  (class A) (McFadden and McElhinny, 1990). Normal polarity ChRM directions are clustered with precision parameter  $k = 181.2$ , with mean  $D = 349.1^\circ$ ,  $I = 64.6^\circ$ , and  $\alpha_{95} = 0.9^\circ$ . For reverse polarity levels, ChRM directions vary significantly ( $k = 10.4$ ), yielding a mean  $D = 176.0^\circ$ ,  $I = -62.5^\circ$  with  $\alpha_{95} = 4.0^\circ$ . The mean normal polarity inclination is close to that for the geocentric axial dipole (GAD) field ( $62.9^\circ$ ) in the study area.

In the 9.00–14.06 m depth interval (Fig. 8), Brunhes normal polarity epoch, virtually no declination and inclination variation is observed. Conversely, in the Matuyama reverse polarity zone (15.80–18.70 m), variations in declination reach  $150^\circ$ , while inclination varies by up to  $55^\circ$ . The cause of these late Matuyama fluctuations is not fully understood. Whether the recorded variations reflect geomagnetic field behavior before the inversion or incomplete VRM removal, remains unclear.

### 3.6. Normalized remanence records

Relative paleointensity (RPI) variations, in addition to

paleomagnetic directions, are a powerful tool for understanding continuous geomagnetic field variations (Tauxe et al., 1995; Channell et al., 2009). RPI can be estimated by applying a pseudo-Thellier approach (Tauxe et al., 1995) or normalizing the natural remanent magnetization by  $\chi$ , ARM, or IRM. To ensure the suitability of sediments for obtaining PRI records, strict reliability criteria are applied (King et al., 1983; Tauxe, 1993). These criteria exclude the influence of magnetostatic interactions and grain size effects on the record. Loess-paleosol sequences rarely satisfy such criteria, however, some RPI records exhibit consistent results (Liu et al., 2015; Pan et al., 2021). Since magnetite is not the only magnetic mineral present in the Otkaznoe LPS, one of the reliability criteria is not satisfied. Therefore, in this paper, we will refer to these records as normalized remanence records instead of RPI records.

We obtained the normalized remanence records using the ratios  $NRM_{300}/\chi$ ,  $NRM_{35MT}/\chi$ ,  $NRM_{35MT}/ARM_{35MT}$  and  $\Delta NRM/\Delta ARM$  (Fig. 9f and g). These ratios have essentially identical variations ( $r = 0.9$ ) with two distinct maxima at 10.80–11.80 m and 17.00–18.00 m, respectively, and a minimum in the depth range from 13.00 to 17.00 m. This minimum corresponds to the M/B transition zone. NRM for the M/B transition is also at least an order of magnitude lower than that for specimens with stable normal or reverse polarity (Fig. 9c).

Normalized remanence records generally align with NRM changes (Fig. 9). The distinct peak at 11.10 m is associated with a magnetic mineral concentration increase (see Section 3.2). The correlation coefficient between these parameters and NRM is 0.73, which is a significant correlation. This supports our hypothesis of incomplete removal of contributions related to concentration and/or size of magnetic grains to the NRM.  $B_c$  and  $B_{cr}$  (Fig. 9d) reveal grain size changes through the

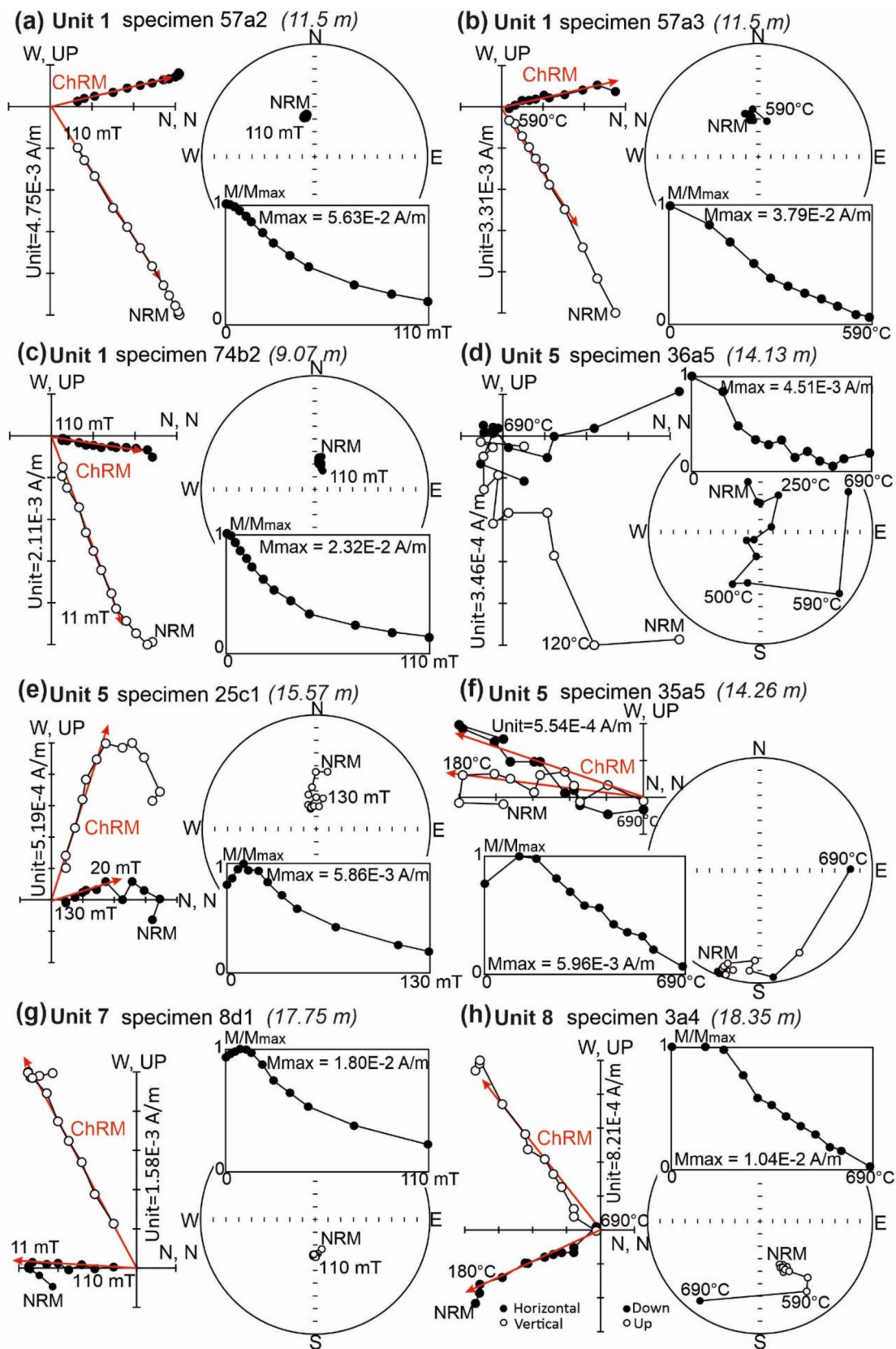


**Fig. 7.** Representative orthogonal (Zijderveld, 1967) vector diagrams, stereograms of component directions and intensity demagnetization plots of alternating field (a, c, e, g) and thermal (b, d, f, h) demagnetization results for normal polarity (a-c), anomalous directions (d-f) and reversal polarity (g-h) samples. Black (white) circles in Zijderveld (1967) diagrams indicate projections on the horizontal (vertical) plane; black (white) circles in stereograms are vector projections on the lower (upper) hemisphere.

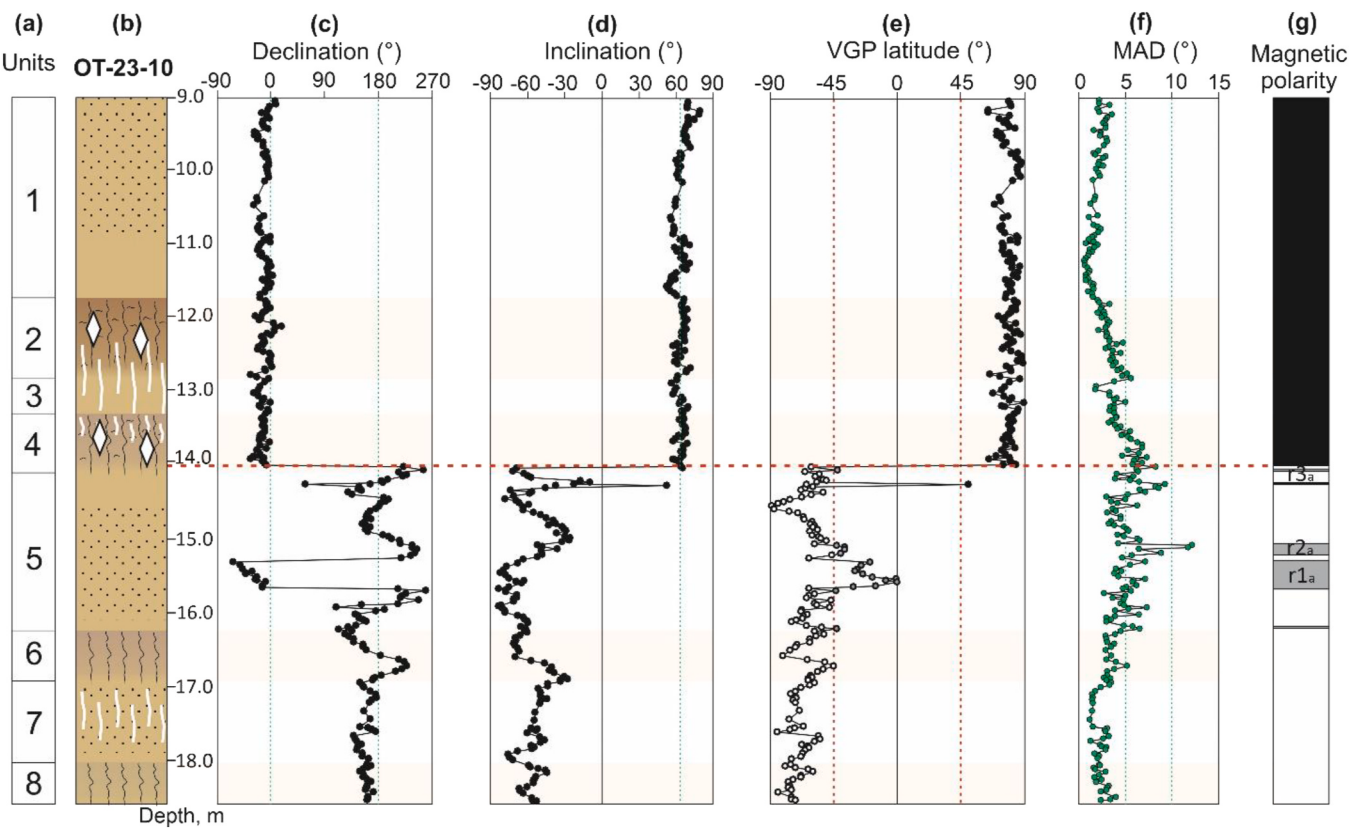


**Fig. 8.** Paleomagnetism of the Otkaznoe section, its (a) lithological units and (b) lithostratigraphy; (c) declination, and (d) inclination. The dashed line represents the expected inclination ( $62.9^\circ$ ) at the latitude of the Otkaznoe section for a geocentric axial dipole (GAD) field; (e) virtual geomagnetic pole (VGP) latitude, (f) maximum angular deviation (MAD); (g) magnetic polarity zones. The Matuyama-Brunhes boundary (MBB) is represented by a red dashed line.

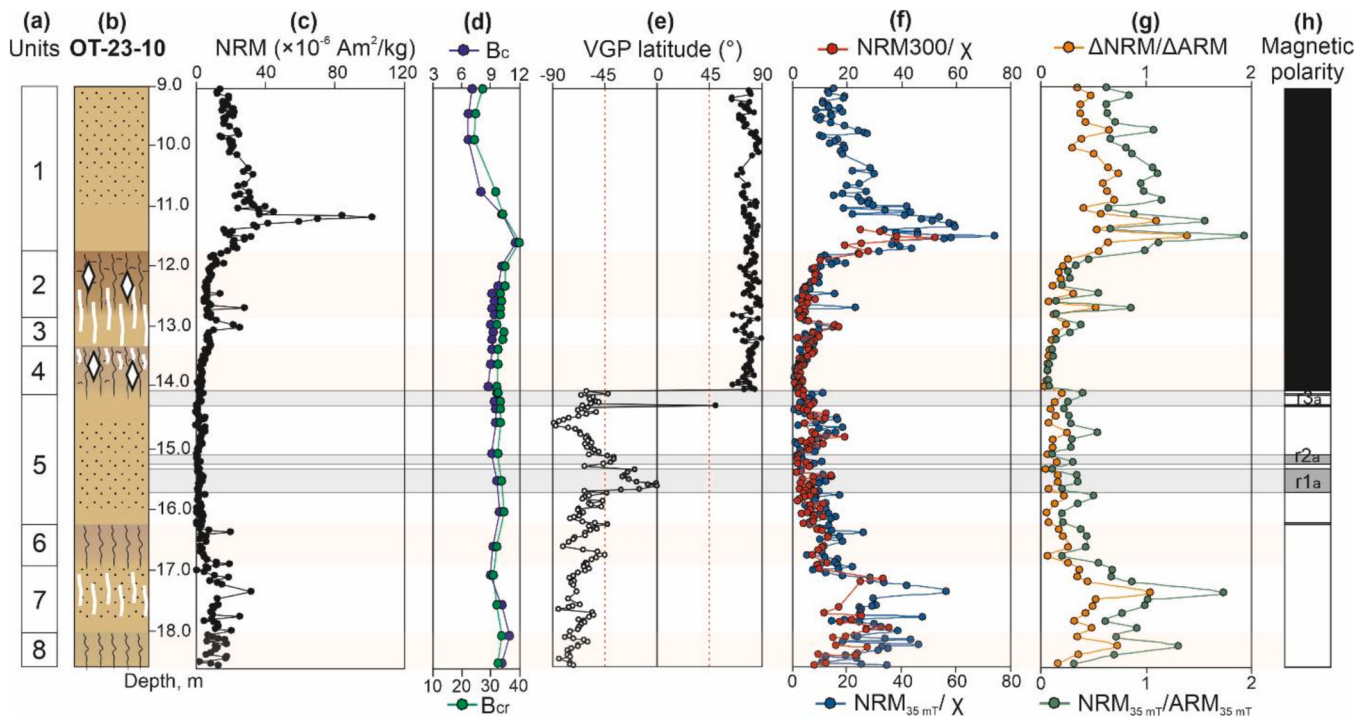


**Fig. 9.** Normalized remanence records across units 1–8 (a) of the Otkaznoe section and (b) its lithostratigraphy: (c) natural remanent magnetization; (d) coercivity ( $B_c$ ) and coercivity of remanence ( $B_{cr}$ ); (e) virtual geomagnetic pole (VGP) latitude; normalized remanence is expressed by (f)  $\text{NRM}_{300}/\chi$ ,  $\text{NRM}_{35\text{mT}}/\chi$  and (g)  $\text{NRM}_{35\text{mT}}/\text{ARM}_{35\text{mT}}$ ,  $\Delta\text{NRM}/\Delta\text{ARM}$ ; (h) magnetic polarity zones.

section. In the interval 11.50–18.70 m,  $B_c$  and  $B_{cr}$  are relatively stable, averaging 9.7 and 33.7 mT, respectively. In contrast, for the upper 2.50 m (9.00–11.50 m),  $B_c$  and  $B_{cr}$  decrease significantly to 7.2 and 27.3 mT, respectively. This reduction may suggest coarser grain size compared to the rest of the section.

Magnetic mineral concentration and grain size variations within the upper 2 m of the section suggest that it is not feasible to accurately assess RPI changes during this interval with NRM normalization. In contrast, stable of the magnetic mineralogy through the rest of section (11.50–18.70 m) supports the hypothesis that low  $NRM_{300}/\chi$ ,  $NRM_{35mT}/\chi$ ,  $NRM_{35mT}/ARM_{35mT}$ , and  $\Delta NRM/\Delta ARM$  between 13.00 and 17.00 m likely indicates low relative paleointensity across the Matuyama-Brunhes transition.

#### 4. Discussion

##### 4.1. Paleomagnetic record of the Matuyama-Brunhes transition in the Otkaznoe loess-paleosol section and comparison with global data

From our data, the MBB in the Otkaznoe section is recorded at the base of unit 4 by a sharp transition from reverse to normal polarity at 14.06 m. The preceding MBB transitional interval, which is 1.74 m thick (14.06–15.80 m), contains individual zones with anomalous paleomagnetic directions (VGP latitude  $\sim 0^\circ$ ) and isolated sharp polarity changes. Also, the NRM and paleomagnetic recording quality are lower compared to periods of stable (normal/reverse) polarity. This indicates a weaker geomagnetic field during reversal.

A VGP path for the Otkaznoe loess-paleosol sequence is shown in Fig. 10. The VGPs related to the Matuyama chron predominantly cluster around Antarctica, while Brunhes chron VGPs are clustered in Arctic latitudes. The transition zone contains single isolated VGPs in both the Southern and Northern Hemispheres around New Zealand and central Eurasia. Also, two distinct VGP clusters are evident to the west and east of South America, corresponding to zones with anomalous paleomagnetic directions r1a and r2a (Fig. 10).

We compare these clusters with VGPs from lavas on La Palma Island ( $N 28^\circ 48'$ ,  $W 17^\circ 47'$ ) with  $^{40}\text{Ar}/^{39}\text{Ar}$  ages close to the M/B precursor (Singer et al., 2002; Camps et al., 2011). As shown in Fig. 10, three poles of Singer et al. (2002) with ages of  $791.2 \pm 18.9$  and  $803.3 \pm 9.3$  ka, align closely with the Otkaznoe VGPs (zones r1a and r2a). These VGPs are located to the west and east of South America, respectively. Similarities between our data and those of Singer et al. (2002) suggest a potential association of zones r1a and r2a with the M/B precursor.

However, these locations are geographically distant from each other, which might suggest a subtle influence of non-dipole magnetic field components.

When comparing VGP clusters from zones r1a and r2a with global data, we consider the Kamikatsura excursion and MBR records of Coe et al. (2004) from lavas at Haleakala, Tahiti ( $N 20^\circ 75'$ ,  $W 156^\circ 22'$ ). VGPs associated with the Kamikatsura event, which has a weighted mean  $^{40}\text{Ar}/^{39}\text{Ar}$  age of  $900.3 \pm 4.7$  ka, form a cluster in near-equatorial latitudes in central South America (Fig. 10). Evans et al. (2011) also discussed the Kamikatsura excursion in the loess-paleosol sequence of Gold Hill (Alaska), where it was identified 160 cm below the Matuyama-Brunhes boundary with VGPs comparable to those reported by Coe et al. (2004). Despite VGP the similarities between the Kamikatsura event and those from zones r1a and r2a (Fig. 10), we suggest that the Kamikatsura excursion is not recorded in the Otkaznoe loess-paleosol section. Given that the age of the Kamikatsura event predates the MBB by at least 100 ka (Channell et al., 2020), interpreting zones r1a and r2a as indicative of the Kamikatsura excursion would suggest a prolonged hiatus during this interval, which is not corroborated by lithological and grain size data (see Section 3.1).

Based on Matuyama-Brunhes transition records from lavas, as well as in marine and lake sediments, Mahgoub et al. (2023) calculated VGP latitudes and RPI variation curves for 11 regions. In Fig. 11, we have shown global VGP and VADM stacks, along with representative VGP latitude curves (Mahgoub et al., 2023; Dinares-Turell et al., 2002; Sagnotti et al., 2014, 2016; Just et al., 2019) from Mediterranean sediment records, the region closest to our study area. In the VGP latitude curve for core ICDP5045-1 ( $N 41.05^\circ$ ,  $E 20.72^\circ$ ) (Fig. 11e) and the global VGP stack (Fig. 11c), a distinct zone with transitional VGPs below  $-45^\circ$  is observed from 785 to 805 ka. This interval has low relative paleointensity and an increase in the paleosecular variation index, which allows quantitative assessment of geomagnetic field stability (Panovska and Constable, 2017). Although the paleomagnetic record from core ICDP5045-1 was not included in global VGP and VADM stacks due to significant differences from the records of Sulmona Basin ( $N 39.31^\circ$ ,  $E 16.34^\circ$ ) and core LC07 ( $N 38.20^\circ$ ,  $E 10.10^\circ$ ) (Mahgoub et al., 2023), it has clear similarities with the Otkaznoe record (Fig. 11a). VGP latitudes for the Otkaznoe section and the global VGP stack in the MBR transitional zone have similar variations (Fig. 11a–c). Furthermore, both the global VADM stack and the normalized remanence records for the Otkaznoe LPS are characterized by a significant decrease during the transition (Fig. 11b–d).

The identified correlations enable us to associate zones r1a and r2a

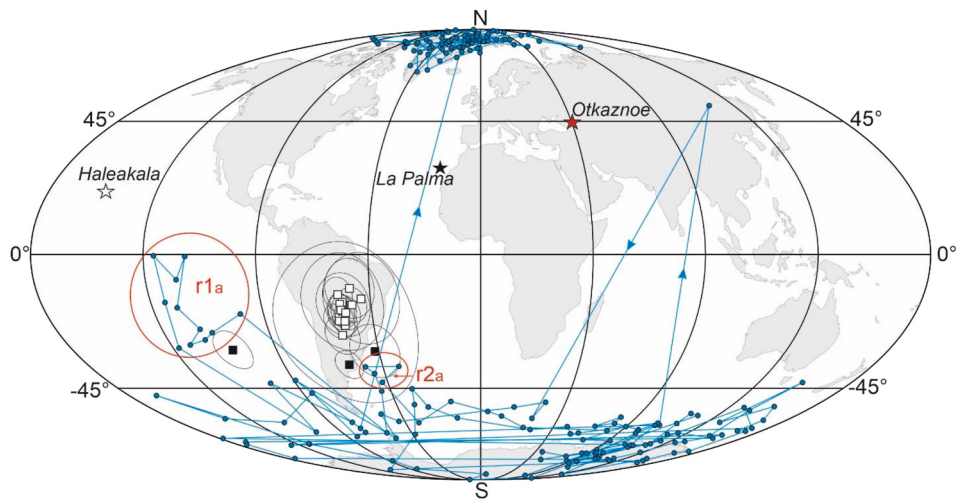


**Fig. 10.** VGP path for the M/B transition for the Otkaznoe section (blue circles), compared to VGPs for the M/B precursor according to Singer et al. (2002) (black squares) and Kamikatsura excursion of Coe et al. (2004) (white squares). Location of the Otkaznoe section is indicated by a red star, La Palma – black star and Haleakala volcano – white star.

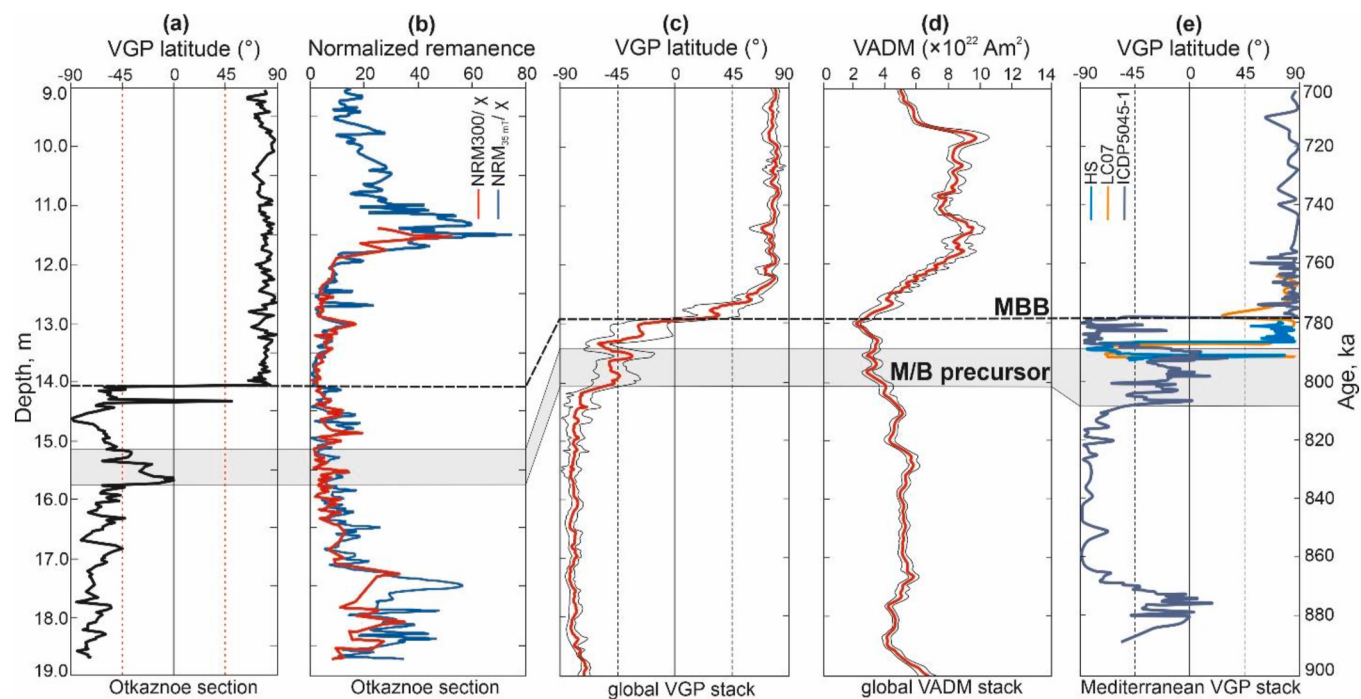


**Fig. 11.** VGP latitude (a) and normalized remanence record (b) for the Otkaznoe section and its correlation with global VGP (c), global VADM (d) and Mediterranean VGP (e) stacks according to Mahgoub et al. (2023).

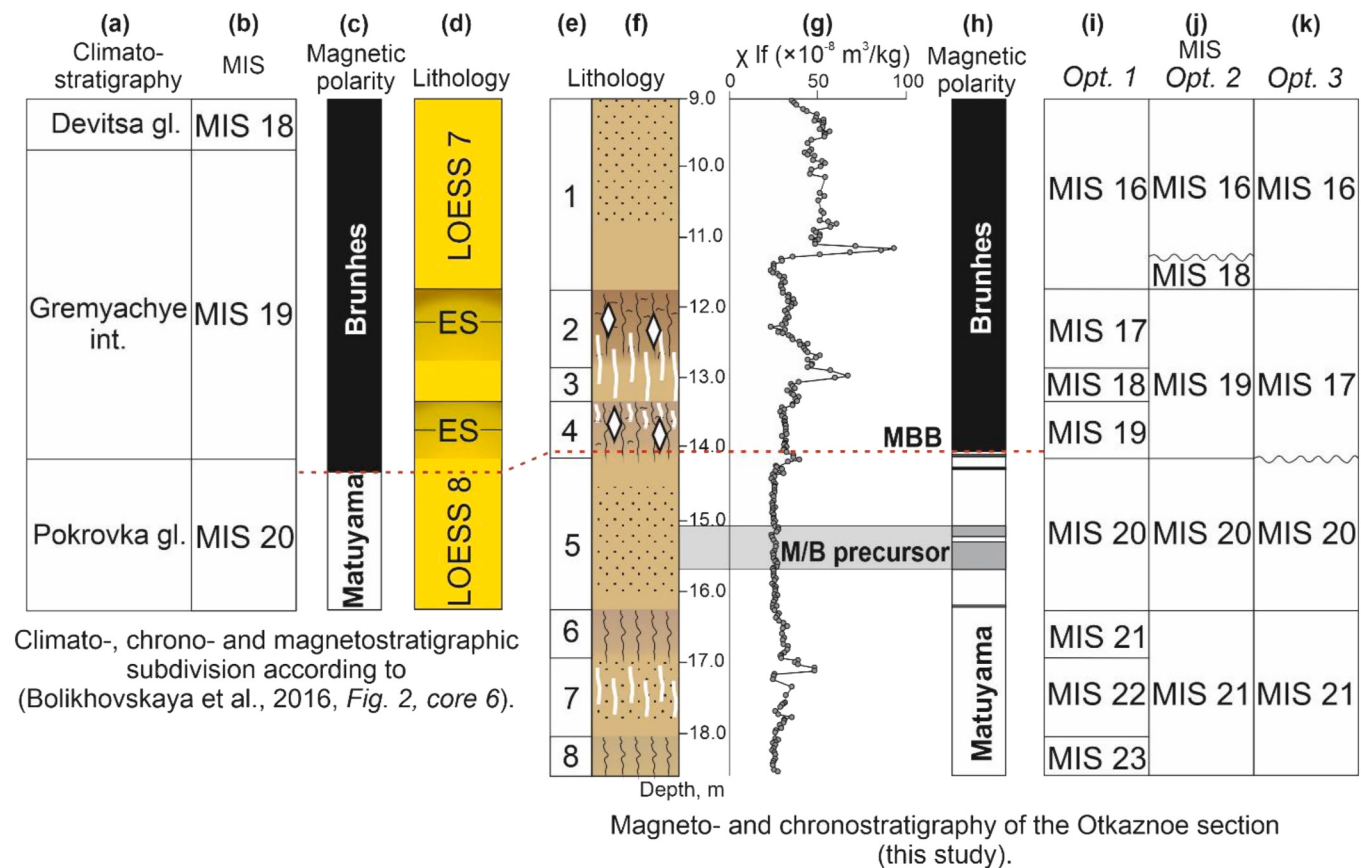


**Fig. 12.** Comparison of chronostratigraphic schemes according to Bolikhovskaya et al. (2016) (a-d) and this study (e-k). ES – embryonic soil. gl. – glacial; int. – interglacial. The Matuyama-Brunhes boundary (MBB) is represented by a red dashed line. Option 2 is the preferred interpretation.

from Otkaznoe section with M/B precursor, while zone r3a can be attributed to the Matuyama-Brunhes boundary. A key question is the chronostratigraphic position of the MBR in this section. Age assessment of loess-paleosol horizons is primarily carried out by correlating magnetic susceptibility variations with the MISs. This is because rock magnetic properties of loess-paleosol deposits, including magnetic susceptibility and its frequency dependence, can reflect global climate fluctuations (Evans and Heller, 2003).

However, as discussed in Section 3.2, units 1–8 do not record the anticipated  $\chi_{lf}$ ,  $\Delta\chi$ , and  $\chi_{fd}$  increase in paleosols compared to loess, which contrasts with loess-paleosol sequences in China. This atypical magnetic susceptibility behavior is likely related not to global paleoclimate fluctuations but to dominant regionally conditioned factors. Chronostratigraphic subdivision of the Otkaznoe section and its linking to MIS should, thus, rely on analysis of pedo-, litho- and magnetostratigraphic data.

#### 4.2. Chronostratigraphy of the Otkaznoe section

Based on field lithological descriptions, grain size, LOI, and magnetic susceptibility analyses for the OT-23-10 LPS, we distinguish 4 paleosol units (Fig. 12e). However, correlation with MIS remains open. We identify two reliable paleomagnetic markers: the M/B precursor and the Matuyama-Brunhes boundary (Fig. 12). The precursor is recorded in loess unit 5 at 15.17–15.80 m, so, we can confidently correlate this loess with MIS 20 (Channell et al., 2020) (Fig. 12i and j). The Matuyama-Brunhes boundary in OT-23-10 occurs at the base of paleosol unit 4 (depth 14.06 m). According to Channell et al. (2020), it corresponds to MIS 19.

If each paleosol and loess horizon corresponds to a single oxygen isotope stage, the OT-23-10 section appears to reflect the MIS 16–23 interval (Fig. 12i). This interpretation implies extremely low accumulation rates during glacial epochs (1.0 cm/ka for MIS 18 and 2.9 cm/ka for MIS 22) and interglacial epochs (1.3–2.4 cm/ka) – while the accumulation rate for MIS 20 is significantly higher (9.2 cm/ka). During extremely low accumulation epochs, it is expected to observe more developed and thicker paleosol profiles (Kemp, 2001). However, at OT-23-10, single paleosols are poorly developed and much thinner compared to the overlying interglacial pedocomplexes. This calls into question option 1 (Fig. 12i).

Grain size is one of most stable sedimentary feature and is sensitive to changes in loess accumulation and soil formation processes (Lu and An, 1998; Vandenberghe, 2013; Velichko et al., 2017; Khmeleva et al., 2022). This allows it to be used to distinguish between loess horizons and pedocomplexes. Units 2–4, which consist of two closely paleosols, are located in a common zone of grain size distribution. The zone is characterized by a low MGS and a high clay content. This is typical for the pedocomplexes of the Otkaznoe LPS, formed during one MIS (Konstantinov et al., 2022). Paleosols belonging to different MIS are usually separated by a layer of low-clay loess with a thickness of several meters or more (Konstantinov et al., 2022; Dudanova et al., 2025). This suggests that the units 2–4 are part of the same pedocomplex, which is supported by increased  $\chi_{lf}$  and  $\chi_{fd}$  at 11.80–14.20 m (Fig. 3c and d). Thus, we propose that units 2–4 accumulated during a single oxygen isotope stage – MIS 19. Accumulation rates during MIS 19 can, thus, be estimated at 7.6 cm/ka. These sedimentation rates are of the same order of magnitude as the rates estimated based on OSL dating (Sychev et al., 2022) for MIS 5 (10 cm/ka) and MIS 1 (9 cm/ka).

By analogy with the upper pedocomplex (units 2–4), we assume that the weakly developed paleosols of units 6 and 8 also belong to the common pedocomplex. Indirect arguments for this are spatial proximity and the assumption of relative constancy of the order of sedimentation rates for paleosols. We classify units 6–8 as a pedocomplex corresponding to MIS 21. While during MIS 21 sedimentation rate was 4.4 cm/ka.

Two key factors that could complicate correlation of loess-paleosol

horizons with MISs should be considered: (1) the potential presence of depositional hiatuses; and (2) delayed remanence acquisition in sediments caused by lock-in processes (Spassov et al., 2003). Sedimentary hiatuses are typical for loess-paleosol sequences, but are difficult to observe, because they are often erased by bioturbation. Nevertheless, recent studies of loess-paleosol sequences in China and Central Asia (Buylaert et al., 2008, 2024), have identified such gaps using luminescence dating with fine resolution. Thus, we can assume the presence of hiatuses in the OT-23-10 section. An apparent hiatus is reflected by a sharp change in lithological (grain size and LOI analyses) and magnetic (magnetic susceptibility and hysteresis properties) records in loess unit 1 at 11.10 m. As shown in Section 3.2, this interval is associated with a magnetic minerals concentration increase, which may indicate a deflation boundary at this depth (Huayu et al., 2006). Based on this interpretation (option 2, Fig. 12j), the thin loess comprising the lower part of unit 1 should correlate with MIS 18, while the sandy loess in upper unit 1 should correspond to the Don loess, which accumulated during MIS 16 (Velichko and Morozova, 2010, 2015). Thus, we propose the absence of a paleosol correlated with MIS 17 (Lisiecki and Raymo, 2005). The hiatus duration can be estimated to be at least 35 ka.

The third option (Fig. 12k) suggests a potential sedimentary hiatus at the boundary between units 4 and 5. This possibility cannot be dismissed, given the abrupt polarity change (MBB) (Fig. 8e). In this case, it can be assumed that the OT-23-10 only recorded the M/B precursor, while the end of the Matuyama-Brunhes transition is absent. In this case, the pedocomplex represented by units 2–4 could correlate with MIS 17, assuming that the loess-paleosol cycle linked to MIS 18–19 was eroded (Fig. 12k). Such a scenario indicates a significant of approximately 80 ka (Lisiecki and Raymo, 2005), which, however, is not revealed from either grain size or LOI analyses. In our view, the most plausible option for correlating loess-paleosol horizons at OT-23-10 with MIS is option 2 (Fig. 12j). In this case, even if there is a hiatus at the boundary between units 4 and 5, it can be assumed that the interrupted sediment accumulation to have been brief.

The polarity transition at the base of unit 4, located at the loess and paleosol boundary, may also be attributed to a lock-in depth effect (Spassov et al., 2003), which leads to a delayed remanence acquisition and downward shifting of paleomagnetic boundaries. Downward shifting of the MBB in MIS 20 (Liu et al., 2015) and even in MIS 21 (Sumegi et al., 2018) is commonly seen in loess-paleosol sequences in China and Europe (Liu et al., 2015; Song et al., 2018). In these instances, the M/B transition zone often has multiple polarity flips, which do not represent true geomagnetic field behavior, rather, they stem from loess remagnetization influenced by pedogenic processes (Spassov et al., 2003). In OT-23-10, the lock-in depth effect is probably present, but it is insignificant due to the relatively low intensity of pedogenic processes.

Our new correlation of the OT-23-10 LPS with marine isotope stages (Lisiecki and Raymo, 2005) differs slightly from composite scheme of Bolikhovskaya et al. (2016) (Fig. 12a–d), which was based primarily on palynological and microtheriological data. Although the lithological descriptions generally coincide (Fig. 12e and f), our data positions the MBB a little higher than indicated by Faustov and Virina (2001) and Bolikhovskaya et al. (2016). Exactly, we highlight the MBB at the base of the MIS 19 paleosol, rather than at the top of the MIS 20 loess.

#### 5. Conclusions

A comprehensive study of the loess-paleosol sequence in the lower Otkaznoe section yielded detailed, high-resolution data, including paleomagnetic, rock magnetic, grain size, loss on ignition records, and X-ray diffraction and scanning electron microscopy analyses, with the first documentation of the Matuyama-Brunhes transition in the Otkaznoe section. The Matuyama-Brunhes reversal in the loess-paleosol sequence of the Otkaznoe section spans a 1.7-m-thick zone with complex structure, incorporating both a precursor to the Matuyama-Brunhes reversal and the Matuyama-Brunhes boundary. This is the first record of

the M/B precursor in the loess-paleosol sections of Europe. The paleomagnetic record of the precursor event makes it a valuable chronostratigraphic marker for regional and global correlations with other sedimentary archives. We also precisely establish the position of the Matuyama-Brunhes boundary in the Otkaznoe loess-paleosol sequence. The Matuyama-Brunhes boundary in the Otkaznoe section is located at the base of the MIS 19 paleosol, rather than in the MIS 20 loess. Our findings suggest that lock-in effects have an insignificant impact on the paleomagnetic record in the Otkaznoe section, unlike in the loess-paleosol sequences of China and Europe. The Otkaznoe sequence provides one of the most comprehensive records of the Matuyama-Brunhes transition among continental deposits on the East European Plain.

#### Author's contributions

Varvara Dudanova: Conceptualization, Methodology, Investigation, Visualization, Writing – Original Draft Preparation, Writing – Review & Editing; Evgeny Konstantinov: Conceptualization, Methodology, Visualization, Writing – Original Draft Preparation, Writing – Review & Editing; Nikita Sychev: Investigation, Visualization, Writing – Original Draft Preparation, Writing – Review & Editing; Aleksandr Pasenko: Methodology, Writing – Review & Editing; Pavel Panin: Investigation,

Writing – Review & Editing; Roman Veselovskiy: Methodology, Writing – Review & Editing.

#### Declaration of competing interest

The authors declare that they have no known competing financial interests or personal relationships that could have appeared to influence the work reported in this paper.

#### Acknowledgements

The research was supported by the state research programs of the IPE RAS FMWU-2025-0033 (rock magnetic and paleomagnetic studies: V. Dudanova, A. Pasenko, R. Veselovskiy), IG RAS FMWS-2024-0003 (field work and lithological analyses: E. Konstantinov, N. Sychev) and IG RAS FMWS-2024-0005 (paleosol research: P. Panin). We thank A. Zakharov, R. Shukhvostov, O. Manakova, F. Kurbanova, V. Wang and M. Khmeleva for participation in field work, N. Afinogenova for performing XRD analyses, and E. Kulakova for valuable insights during data interpretation. We thank A.P. Roberts and anonymous reviewer for their thorough review and constructive comments.

#### Appendix A. Supplementary data

Supplementary data to this article can be found online at <https://doi.org/10.1016/j.quascirev.2025.109628>.

#### Appendices.

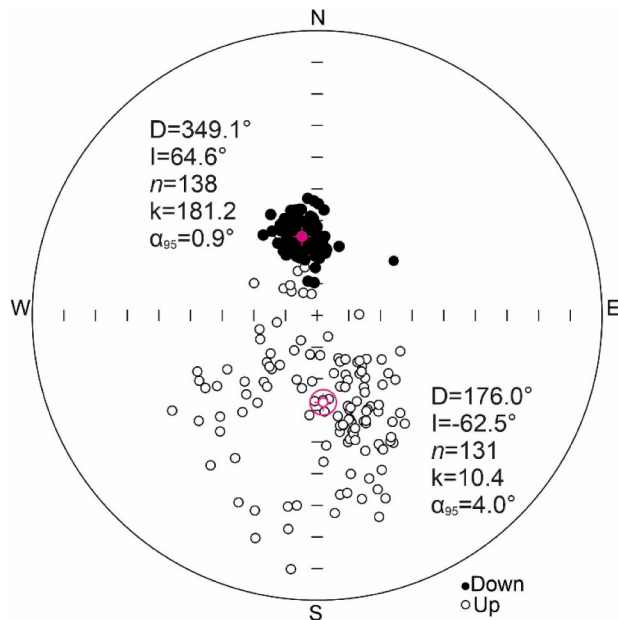


**Fig. A.1.** Stereogram of the average ChRM direction distribution for each stratigraphic level.

#### Data availability

A link to the data and/or code is provided as part of this submission.

#### References

- Alekseev, A.O., Alekseeva, T.V., 2024. Mineralogy and magnetic properties of the loess-soil formation as the reflection of the landscape and climatic conditions in the Terek-Kuma Lowland in the Pleistocene. *Eurasian Soil Sci.* 57 (1), 63–73. <https://doi.org/10.1134/S1064229323602457>.  
 Andreeva, T.V., Trofimov, V.T., Shaevich, Ya E., 2008. In: Trofimov, V.T. (Ed.), *Reference Engineering-Geological Sections of Loess in the European Region of Russia*, pp. 173–314 (in Russian).  
 Beget, J.E., Hawkins, D.B., 1989. Influence of orbital parameters on Pleistocene loess deposits in Central Alaska. *Nature* 337, 151–153. <https://doi.org/10.1038/337151a0>.  
 Bengtsson, L., Enel, M., 1986. Chemical analysis. In: *Handbook of Holocene Palaeoecology and Palaeohydrology*. John Wiley & Sons, Chicago, pp. 423–451.

- Blott, S.J., Croft, D.J., Pye, K., Saye, S.E., Wilson, H.E., 2004. Particle size analysis by laser diffraction. Geological Society, London, Special Publications 232 (1), 63–73. <https://doi.org/10.1144/gsl.sp.2004.232.01.08>.
- Bradak, B., Kovacs, J., Magyari, A., 2019. The origin and significance of some ‘irregular’ loess magnetic fabric found in the Paks succession (Hungary). *Geophys. J. Intell.* 217 (3), 1742–1754. <https://doi.org/10.1093/gji/ggj117>.
- Bradak, B., Seto, Yu., Stevens, Th., Ujvari, G., Feher, K., 2021. Magnetic susceptibility in the European Loess Belt: new and existing models of magnetic enhancement in loess. *Palaeogeogr. Palaeoclimatol. Palaeoecol.* 569, 110329. <https://doi.org/10.1016/j.palaeo.2021.110329>.
- Bolikhovskaya, N.S., 1995. *The Evolution of the Loess-Paleosol Formation of the Northern Eurasia*. Moscow State University Press, Moscow, p. 270 (in Russian).
- Bolikhovskaya, N.S., Faustov, S.S., Markova, A.K., 2016. Pleistocene climatic stratigraphy and environments of the Terek-Kuma Lowland (NW Caspian Sea region) inferred from palynological, paleomagnetic and rodent records of the long Otkaznoye sediment sequence. *Quat. Int.* 409 (A), 16–32. <https://doi.org/10.1016/j.quaint.2015.09.067>.
- Bronger, A., 2003. Correlation of loess–paleosol sequences in East and Central Asia with SE Central Europe: towards a continental Quaternary pedostratigraphy and paleoclimatic history. *Quat. Int.* 106–107, 11–31. [https://doi.org/10.1016/S1040-6182\(02\)00159-3](https://doi.org/10.1016/S1040-6182(02)00159-3).
- Buylaert, J.P., Murray, A.S., Vandenberghe, D., Vriend, M., Corte, F. De, Van den Haute, P., 2008. Optical dating of Chinese loess using sand-size quartz: establishing a time frame for Late Pleistocene climat changes in the western part of the Chinese Loess Plateau. *Quat. Geochronol.* 3 (1–2), 99–113. <https://doi.org/10.1016/j.quageo.2007.05.003>.
- Buylaert, J.P., Challier, A., Kulakova, E.P., Taratunina, N.A., Thomsen, K.J., Utkina, A.O., Sosin, P.M., Tokareva, O.A., Anoikin, A.A., Khujageldiev, T.U., 2024. A luminescence dating study the upper part of loess–paleosol sequence at Kuldara, Khovaling Loess Plateau, Tajikistan. *Quat. Geochronol.* 82, 101545. <https://doi.org/10.1016/j.quageo.2024.101545>.
- Camps, P., Singer, B.S., Carvallo, C., Goguitchaichvili, A., Fanjat, G., Allen, B., 2011. The Kamiksutra event and the Matuyama–Brunhes reversal recorded in lavas from Tjornes Peninsula, Northern Iceland. *Earth Planet Sci. Lett.* 310 (1–2), 33–44. <https://doi.org/10.1016/j.epsl.2011.07.026>.
- Channell, J., Xuan, C., Hodell, D., 2009. Stacking paleointensity and oxygen isotope data for the last 1.5 Myr (PISO-1500). *Earth Planet Sci. Lett.* 283 (1–4), 14–23. <https://doi.org/10.1016/j.epsl.2009.03.012>.
- Channell, J.E.T., Singer, B.S., Jicha, B.R., 2020. Timing of Quaternary geomagnetic reversals and excursions in volcanic and sedimentary archives. *Quat. Sci. Rev.* 228, 106114. <https://doi.org/10.1016/j.quascirev.2019.106114>.
- Coe, R.S., Singer, B.S., Pringle, M.S., Zhao, X., 2004. Matuyama–Brunhes reversal and Kamiksutra event on Maui: paleomagnetic directions,  $^{40}\text{Ar}/^{39}\text{Ar}$  ages and implications. *Earth Planet Sci. Lett.* 222 (2), 667–684. <https://doi.org/10.1016/j.epsl.2004.03.003>.
- Cosentino, N.J., Torre, G., Lambert, F., Albani, S., De Vleeschouwer, F., Bory, m., 2024. Paleo±Dust: quantifying uncertainty in paleo-dust deposition across archive types. *Earth Syst. Sci. Data* 16, 941–959. <https://doi.org/10.5194/essd-16-941-2024>.
- Dean, W.E., 1974. Determination of carbonate and organic matter in calcareous sediments and sedimentary rocks by loss on ignition; comparison with other methods. *J. Sediment. Res.* 44 (1), 242–248. <https://doi.org/10.1306/74d729d2-2b21-11d7-8648000102c1865d>.
- Deng, Ch., Zhu, R., Verosub, K.L., Singer, M.J., Yuan, B., 2000. Paleoclimatic significance of the temperature-dependent susceptibility of Holocene loess along a NW-SE transect in the Chinese loess plateau. *Geophys. Res. Lett.* 27 (22), 3715–3718. <https://doi.org/10.1029/2000GL008462>.
- Dinares-Turrell, J., Sagnotti, L., Roberts, A.P., 2002. Relative geomagnetic paleointensity from the Jaramillo subchron at the Matuyama–Brunhes boundary as recorded in a Mediterranean piston core. *Earth Planet Sci. Lett.* 194 (3–4), 327–341. [https://doi.org/10.1016/s0012-821x\(01\)00563-5](https://doi.org/10.1016/s0012-821x(01)00563-5).
- Dodonov, A.E., 1991. Loess of central Asia. *Geojournal* 24. <https://doi.org/10.1007/BF00186015>.
- Dudanova, V.I., Konstantinov, E.A., Pasenko, A.M., Sychev, N.V., Veselovskyi, R.V., 2025. Big Lost geomagnetic excursion recorded in the loess-paleosol sequence in the Southern part of European Russia, Otkaznoye section. *Dokl. Earth Sci.* 522 (45). <https://doi.org/10.1134/S1028334X25606455>.
- Fremov, I.V., Veselovskyi, R.V., 2023. PMTools: new application for paleomagnetic data analysis. *Izvestiya Phys. Solid Earth* 59, 798–805. <https://doi.org/10.1134/S1069351323050026>.
- Evans, M., Heller, F., 2003. *Environmental magnetism: Principles and applications of environmental magnetism*. Int. Geophys. Ser. Academic Press, p. 299.
- Evans, M.E., Jensen, B.J.L., Kravchinsky, V.A., Froese, D.G., 2011. The Kamiksutra event in the Gold Hill, Alaska. *Geophys. Res. Lett.* 38 (13). <https://doi.org/10.1029/2011GL047793>.
- Fan, Y., Cai, S., Pavon-Carrasco, F.J., Xiong, J., Deng, C., Pan, Y., 2024. High-resolution paleomagnetic secular variation since ~13 ka from a loess section in Northwest China and a regional geomagnetic directional model for East Asia. *J. Geophys. Res.* 129 (4), e2023JB028094. <https://doi.org/10.1029/2023JB028094>.
- Faustov, S.S., Virina, E.I., 2001. The stratigraphic position of Matuyama–Brunhes boundary in loess formation of the Russian Plain. *Bulletin of Commission for study of the Quaternary* 64, 21–31 (in Russian).
- Fisher, R.A., 1953. Dispersion on a sphere. *Proceedings of the Royal Society. A Mathematical, Physical and Engineering Sciences* 217 (1130), 295–305.
- Galay, B.F., 1992. *Lithogenesis and Subsidence of Aeolian Loesses (By the Example of the Central Caucasian Forelands)*. Abstract of doctoral thesis. Moscow, 39 (in Russian).
- Gates-Rector, S., Blanton, T., 2019. The powder diffraction file: a quality materials characterization database. *Powder Diffir.* 34 (4), 352–360. <https://doi.org/10.1017/S0885715619000812>.
- Ge, J., Guo, Zh., Zhao, D., Zhang, Yi., Wang, T., Yi, L., Deng, Ch., 2014. Spatial variations in paleowind direction during the last glacial period in north China reconstructed from variations in the anisotropy of magnetic susceptibility of loess deposits. *Tectonophysics* 629, 353–361. <https://doi.org/10.1016/j.tecto.2014.07.002>.
- Heiri, O., Lotter, A.F., Lemcke, G., 2001. Loss on ignition as a method for estimating organic and carbonate content in sediments: reproducibility and comparability of results. *J. Paleolimnol.* 25, 101–110. <https://doi.org/10.1023/A:1008119611481>.
- Heller, F., Shen, C.D., Beer, J., Liu, X.M., Liu, T.S., Bronger, A., Suter, M., Bonani, G., 1993. Quantitative estimates and palaeoclimatic implications of pedogenic ferromagnetic mineral formation in Chinese loess. *Earth Planet Sci. Lett.* 114, 385–390. [https://doi.org/10.1016/0012-821X\(93\)90038-B](https://doi.org/10.1016/0012-821X(93)90038-B).
- Huayu, L., Stevens, Th., Shuangwen, Y., Xuefeng, S., 2006. An erosional hiatus in Chinese loess sequences revealed by closely spaced optical dating. *Chin. Sci. Bull.* 51 (18), 2253–2259. <https://doi.org/10.1007/s11434-006-2097-x>.
- Jelinek, V., 1981. Characterization of the magnetic fabric of rocks. *Tectonophysics* 79 (3–4), T63–T67. [https://doi.org/10.1016/0040-1951\(81\)90110-4](https://doi.org/10.1016/0040-1951(81)90110-4).
- Just, J., Sagnotti, L., Nowaczyk, N.R., Francke, A., Wagner, B., 2019. Recordings of fast paleomagnetic reversals in a 1.2 Ma greigite-rich sediment archive from Lake Ohrid, Balkans. *J. Geophys. Res.* 124 (12), 12445–12464. <https://doi.org/10.1029/2019jb018297>.
- Kalinin, P.I., Zanina, O.G., Panin, P.G., Kudrevatykh, I.Yu., 2024. Phytolithic and Paleolandscape evidences of environmental change in the south of the East-European plain in the pleistocene. *Eurasian Soil Sci.* 57, 74–85. <https://doi.org/10.1134/S1064229323602494>.
- Kemp, R.A., 2001. Pedogenic modification of loess: significance for palaeoclimatic reconstructions. *Earth Sci. Rev.* 54 (1–3), 145–156. [https://doi.org/10.1016/S0012-8252\(01\)00045-9](https://doi.org/10.1016/S0012-8252(01)00045-9).
- Khmeleva, M.V., Panin, P.G., Chepalyga, A.L., Karpukhina, N.V., Naidina, O.D., Bukhonov, A.V., 2022. The structure and formation conditions of the early Pleistocene paleosols in the loess-paleosol sequence of the Alchak-Sedlovina section (Republic of Crimea). *Geomorphologiya* 53, 89–102. <https://doi.org/10.31857/S0435428122050054>.
- King, J.W., Banerjee, S.K., Marvin, J., 1983. A new rock magnetic approach to selecting sediments for geomagnetic paleointensity studies: application to paleointensity for the last 4000 years. *J. Geophys. Res.* 88, 5911–5921.
- Kirschvink, J.L., 1980. The least-squares line and plane and the analysis of palaeomagnetic data. *Geophys. J. Int.* 62 (3), 699–718. <https://doi.org/10.1111/j.1365-246X.1980.tb02601.x>.
- Konert, M., Vandenberghe, J.E.F., 1997. Comparison of laser grain size analysis with pipette and sieve analysis: a solution for the underestimation of the clay fraction. *Sedimentology* 44 (3), 523–535. <https://doi.org/10.1046/j.1365-3091.1997.d01-38.x>.
- Konstantinov, E.A., Zakharov, A.L., Sychev, N.V., Mazneva, E.A., Kurbanov, R.N., Morozova, P.A., 2022. Loess accumulation in the southern part of European Russia at the end of the Quaternary Period. *Herald Russ. Acad. Sci.* 92, 342–351. <https://doi.org/10.1134/s1019316222030108>.
- Kukla, G., An, Z., 1989. Loess stratigraphy in Central China. *Palaeogeogr. Palaeoclimatol. Palaeoecol.* 72, 203–225. [https://doi.org/10.1016/0031-0182\(89\)90143-0](https://doi.org/10.1016/0031-0182(89)90143-0).
- Kulakova, E., Kurbanov, R., 2023. First paleomagnetic record of the Matuyama–Brunhes transition in the loess-paleosol series of Tajikistan. In: Kostrov, A., Lyskova, E., Mironova, I., Apatenkov, S., Baranov, S. (Eds.), *Problems of Geocosmos—2022. ICS 2022. Springer Proceedings in Earth and Environmental Sciences*. Springer, Cham. [https://doi.org/10.1007/978-3-031-40728-4\\_6](https://doi.org/10.1007/978-3-031-40728-4_6).
- Lagroix, F., Banerjee, S.K., 2004. The regional and temporal significance of primary aeolian magnetic fabrics preserved in Alaskan loess. *Earth Planet Sci. Lett.* 225, 379–395. <https://doi.org/10.1016/j.epsl.2004.07.003>.
- Lisiecki, L.E., Raymo, M.E., 2005. A Pliocene–Pleistocene stack of 57 globally distributed benthic  $\delta^{18}\text{O}$  records. *Paleoceanography* 20 (1). <https://doi.org/10.1029/2004PA001071>. PA 1003.
- Liu, X.M., Hesse, P., Ralph, T., Beget, J.E., 1999. Properties of magnetic mineralogy of Alaskan loess: evidence for pedogenesis. *Quat. Int.* 62 (1), 93–102. [https://doi.org/10.1016/S1040-6182\(99\)00027-0](https://doi.org/10.1016/S1040-6182(99)00027-0).
- Liu, Q., Jackson, M.J., Banerjee, S.K., Maher, B.A., Deng, Ch., Pan, Yo., Zhu, R., 2004. Mechanism of the magnetic susceptibility enhancements of the Chinese loess. *J. Geophys. Res. Solid Earth* 109 (B12). <https://doi.org/10.1029/2004JB003249>.
- Liu, X., Liu, T., Hesse, P., Xia, D., Chlachula, J., Guan, W., 2008. Two pedogenic models for paleoclimatic records of magnetic susceptibility from Chinese and Siberian loess. *Sci. China Earth Sci.* 51, 284–293. <https://doi.org/10.1007/s11430-007-0145-2>.
- Liu, Q., Jin, Ch., Hu, P., Jiang, Zh., Ge, K., Roberts, A.P., 2015. Magnetostratigraphy of Chinese loess-paleosol sequences. *Earth Sci. Rev.* 150, 139–167. <https://doi.org/10.1016/j.earscirev.2015.07.009>.
- Lu, H., An, Z., 1998. Paleoclimatic significance of grain size of loess-paleosol deposit in Chinese Loess Plateau. *Sci. China Earth Sci.* 41 (6), 626–631.
- Maher, B.A., 2011. The magnetic properties of Quaternary aeolian dusts and sediments, and their palaeoclimatic significance. *Aeolian Research* 3, 87–144. <https://doi.org/10.1016/j.aeolia.2011.01.005>.
- Maher, B.A., 2016. Palaeoclimatic records of the loess/palaeosol sequences of the Chinese Loess Plateau. *Quat. Sci. Rev.* 154, 23–84. <https://doi.org/10.1016/j.quascirev.2016.08.004>.
- Mahgoub, A.N., Korte, M., Panovska, S., 2023. Characteristics of the Matuyama–Brunhes magnetic field reversal based on a global data compilation. *J. Geophys. Res.* 128, e2022JB025286. <https://doi.org/10.1029/2022JB025286>.

- Marković, S.B., Stevens, T., Mason, J., Vandenberghe, J., Yang, S., Veres, D., Lehmkühl, F., 2018. Loess correlations – between myth and reality. *Palaeogeogr. Palaeoclimatol. Palaeoecol.* 509, 4–23. <https://doi.org/10.1016/j.palaeo.2018.04.018>.
- Mazneva, E., Konstantinov, E., Zakharov, A., Sychev, N., Tkach, N., Kurbanov, R., Sedaeva, K., Murray, A., 2021. Middle and late pleistocene loess of the Westn Ciscaucasia: stratigraphy, lithology and composition. *Quat. Int.* 590, 146–163. <https://doi.org/10.1016/j.quaint.2020.11.039>.
- McFadden, P.L., McElhinny, M.W., 1990. Classification of the reversal test in palaeomagnetism. *Geophys. J. Int.* 103 (3), 725–729. <https://doi.org/10.1111/j.1365-246X.1990.tb05683.x>.
- Morozov, D.R., 1989. Micromorphological Features of Pleistocene Soil Formation in the Eastern Ciscaucasia, vol. 51. Bulletin of V.V. Dokuchaev Institute of Soils, pp. 21–24 (In Russian).
- Niezabitowska, D., Stevens, Th., Bradák, B., Chadima, M., Baykal, Yu., Sechi, D., Schneider, R., 2024. Mineral magnetism and palaeoenvironment recorded in loess in southern England. *J. Quat. Sci.* 39 (5), 710–728. <https://doi.org/10.1002/jqs.3620>.
- Ozer, M., Orhan, M., Isik, N.S., 2010. Effect of particle optical properties on size distribution of soils obtained by laser diffraction. *Environ. Eng. Geosci.* 16 (2), 163–173. <https://doi.org/10.2113/gseegeoisci.16.2.163>.
- Pan, Q., Xiao, G., Zhao, Q., Chen, R., Ao, H., Shen, Y., Cheng, J., Zhu, Z., 2021. The Jaramillo subchron in Chinese loess-paleosol sequences. *Palaeogeogr. Palaeoclimatol. Palaeoecol.* 572, 110423. <https://doi.org/10.1016/j.palaeo.2021.110423>.
- Panin, P.G., Timireva, S.N., Morozova, T.D., Kononov, YuM., Velichko, A.A., 2018. Morphology and micromorphology of the loess-paleosol sequences in the south of the East European plain (MIS 1–MIS 17). *Catena* 168, 79–101. <https://doi.org/10.1016/j.catena.2018.01.032>.
- Panin, P., Kalinin, P., Filippova, K., Sychev, N., Bukhonov, A., 2023. Paleo-pedological record in loess deposits in the south of the East European plain, based on Beglitsa-2017 section study. *Geoderma* 437, 116567. <https://doi.org/10.1016/j.geoderma.2023.116567>.
- Panovska, S., Constable, C., 2017. An activity index for geomagnetic paleosecular variation, excursions, and reversals. *G-cubed* 18 (4), 1366–1375. <https://doi.org/10.1002/2016gc006668>.
- Ponomareva, V., Portnyagin, M., Danisk, M., Konstantinov, E., Zelenin, E., Tkach, N., et al., 2023. Distal tephras along the SE European margin date powerful explosive eruptions from the Elbrus volcanic center (Greater Caucasus). *Quat. Sci. Rev.* 300, 107910. <https://doi.org/10.1016/j.quascirev.2022.107910>.
- Pye, K., 1995. The nature, origin and accumulation of loess. *Quat. Sci. Rev.* 14 (7–8), 653–667. [https://doi.org/10.1016/0277-3791\(95\)00047-X](https://doi.org/10.1016/0277-3791(95)00047-X).
- Sagnotti, L., Scardia, G., Giaccio, B., Liddicoat, J.C., Nomade, S., Renne, P.R., Sprain, C. J., 2014. Extremely rapid directional change during Matuyama-Brunhes geomagnetic polarity reversal. *Geophys. J. Int.* 199 (2), 1110–1124. <https://doi.org/10.1093/gji/ggi287>.
- Sagnotti, L., Giaccio, B., Liddicoat, J.C., Nomade, S., Renne, P.R., Scardia, G., Sprain, C. J., 2016. How fast was the Matuyama–Brunhes geomagnetic reversal? A new subcentennial record from the Sulmona basin, central Italy. *Geophys. J. Int.* 204 (2), 798–812. <https://doi.org/10.1093/gji/ggv486>.
- Singer, B.S., Relle, M.R., Hoffman, K.A., Battle, A., Guillou, H., Laj, C., Carracedo, J.C., 2002. Ar/Ar ages of transitionally magnetized lavas on La Palma, Canary Islands, and the geomagnetic instability timescale. *J. Geophys. Res.* 107 (B11), 2307. <https://doi.org/10.1029/2001JB001613>.
- Singer, B., Jicha, B.R., Mochizuki, N., Coe, R.S., 2019. Synchronizing volcanic, sedimentary, and ice core records of Earth's last magnetic polarity reversal. *Sci. Adv.* 5 (8), eaaw4621. <https://doi.org/10.1126/sciadv.aaw4621>.
- Song, Ya., Guo, Zh., Marovic, S., Hambach, U., Deng, Ch., Chang, L., Wu, J., Hao, Q., 2018. Magnetic stratigraphy of the Danube loess: a composite Titel-Stari Slankamen loess section over the last one million years in Vojvodina, Serbia. *J. Asian Earth Sci.* 155, 68–80. <https://doi.org/10.1016/j.jseaes.2017.11.012>.
- Spassov, S., Heller, F., Evans, M.E., Yue, L.P., Dobeneck, T., 2003. A lock-in model for the complex Matuyama–Brunhes boundary record of the loess/paleosol sequence at Lingtai (Central Chinese Loess Plateau). *Geophys. J. Int.* 155 (2), 350–366. <https://doi.org/10.1046/j.1365-246X.2003.02026.x>.
- Sumegi, P., Gulyás, S., Molnar, D., Sumegi, B.P., Almond, P.C., Vandenberghe, J., 2018. New chronology of the best developed loess/paleosol sequence of Hungary capturing the past 1.1 ma: implications for correlation and proposed pan-Eurasian stratigraphic schemes. *Quat. Sci. Rev.* 191, 144–166. <https://doi.org/10.1016/j.quascirev.2018.04.012>.
- Sychev, N.V., Konstantinov, E.A., Zakharov, A.L., Frechen, M., Tsukamoto, S., 2022. New data on geochronology of the upper quaternary loess-soil series in the Terek-Kuma Lowland. *Lithol. Miner. Resour.* 57, 336–347. <https://doi.org/10.1134/S0024490222040071>.
- Tauxe, L., 1993. Sedimentary records of relative paleointensity of the geomagnetic field: theory and practice. *Rev. Geophys.* 36.
- Tauxe, L., Pick, T., Kok, Y.S., 1995. Relative paleointensity in sediments: a pseudo-thellier approach. *Geophys. Res. Lett.* 22 (21), 2885–2888. <https://doi.org/10.1029/95GL03166>.
- Tauxe, L., 2010. Essentials of paleomagnetism. *Geol. Mag.* 147 (6), 489. <https://doi.org/10.1017/S0016756810000555>. Berkeley: University of California Press.
- Tsatskin, A., Heller, F., Hailwood, E.A., Gendler, T.S., Hus, J., Montgomery, P., Sartori, M., Virina, E.I., 1998. Pedosedimentary division, rock magnetism and chronology of the loess/paleosol sequence at Roxolany (Ukraine). *Palaeogeogr. Palaeoclimatol. Palaeoecol.* 143, 111–133. [https://doi.org/10.1016/S0031-0182\(98\)00073-X](https://doi.org/10.1016/S0031-0182(98)00073-X).
- Udartsev, V.P., Bolikhovskaya, N.S., Virina, E.I., 1989. Reference sections, chronostratigraphy and paleogeography of the loess sediments of Ciscaucasian loess region. *Engineering Geology of the Loess Deposits* 2, 102–103 (In Russian).
- Valet, J.-P., Fournier, A., Courtillot, V., Herrero-Bervera, E., 2012. Dynamical similarity of geomagnetic field reversals. *Nature* 490 (7418), 89–93. <https://doi.org/10.1038/nature11491>.
- Vandenberghe, J., 2013. Grain size of fine-grained windblown sediment: a powerful proxy for process identification. *Earth Sci. Rev.* 121, 18–30. <https://doi.org/10.1016/j.earscirev.2013.03.001>.
- Varga, G., Újvári, G., Kovács, J., 2019. Interpretation of sedimentary (sub)populations extracted from grain size distributions of Central European loess-paleosol series. *Quat. Int.* 502, 60–70. <https://doi.org/10.1016/j.quaint.2017.09.021>.
- Velichko, A.A., 1990. Loess-paleosol formation on the Russian plain. *Quat. Int.* 7–8, 103–114. [https://doi.org/10.1016/1040-6182\(90\)90044-5](https://doi.org/10.1016/1040-6182(90)90044-5).
- Velichko, A.A., Morozova, T.D., Panin, P.G., 2007. Polygenetic soil complexes as systematic phenomena of Pleistocene macrocycles. *Izvestiya RAN. Ser. Geograf.* 2, 44–54 (In Russian).
- Velichko, A.A., Morozova, T.D., 2010. Basic features of late pleistocene soil formation in the east european plain and their paleogeographic interpretation. *Eurasian Soil Sci.* 43, 1535–1546. <https://doi.org/10.1134/S1064229310130120>.
- Velichko, A.A., Morozova, T.D., 2015. Main features of soil formation within the Pleistocene on the East European Plain and their paleogeographical. In: Kudryarov, V.N., Ivanov, I.V. (Eds.), *Evolution of Soil and Soil Cover. Theory, Diversity of Natural Evolution and Anthropogenic Transformations of Soil*. GEOS, Moscow, pp. 321–337 (In Russian).
- Velichko, A., Morozova, T.D., Borisova, O.K., Timireva, S.N., Semenov, V.V., Kononov, Yu M., Titov, V., Tesakov, A.S., Konstantinov, E.A., Kurbanov, R.N., 2012. Development of the steppe zone in southern Russia based on the reconstruction from the loess-soil formation in the Don-Azov Region. *Dokl. Earth Sci.* 445, 999–1002. <https://doi.org/10.1134/S1028334X12080107>.
- Velichko, A.A., Borisova, O.K., Kononov, YuM., Konstantinov, E.A., Kurbanov, R.N., Morozova, T.D., Panin, P.G., Semenov, V.V., Tesakov, A.S., Timireva, S.N., Titov, V. V., Frolov, P.D., 2017. Reconstruction of Late Pleistocene events in the periglacial area in the southern part of the East European Plain. *Dokl. Earth Sci.* 475, 895–899. <https://doi.org/10.1134/S1028334X17080098>.
- Veselovsky, R.V., Dubinya, N.V., Ponomarev, A.V., Fokin, I.V., Patonin, A.V., Pasenko, A.M., 2022. Shared research Facilities “petrophysics, geomechanics and paleomagnetism” of the Schmidt Institute of Physics of the Earth RAS. *Geodynamics & Tectonophysics* 13 (2), 579. <https://doi.org/10.5800/GT-2022-13-2-0579>.
- Zhang, R., Kravchinsky, V.A., Zhu, R., Yue, L., 2010. Paleomonsoon route reconstruction along a W-E transect in the Chinese Loess Plateau using the anisotropy of magnetic susceptibility: Summer monsoon model. *Earth Planet Sci. Lett.* 299 (3–4), 436–446. <https://doi.org/10.1016/j.epsl.2010.09.026>.
- Zhu, R., Liu, Q., Jackson, M.J., 2004. Paleoenvironmental significance of the magnetic fabrics in Chinese loess-paleosols since the last interglacial (<130 ka). *Earth Planet Sci. Lett.* 221 (1–4), 55–69. [https://doi.org/10.1016/S0012-821X\(04\)00103-7](https://doi.org/10.1016/S0012-821X(04)00103-7).
- Zijderveld, J.D.A., 1967. AC demagnetization of rocks: analysis of results. In: Runcorn, S. K., Creer, K.M., Collinson, D.W. (Eds.), *Methods in Palaeomagnetism*. Elsevier, Amsterdam, pp. 254–286.